

International Atomic Energy Agency

INDC(CCP)-229/L

---

**INDC**


**INTERNATIONAL NUCLEAR DATA COMMITTEE**

---

TRANSLATIONS OF SELECTED PAPERS PUBLISHED IN

NUCLEAR CONSTANTS 1(50) 1983

(Russian original distributed as INDC(CCP)-213/G)

  
Translated by the IAEA

November 1984

---

**IAEA NUCLEAR DATA SECTION, WAGRAMERSTRASSE 5, A-1400 VIENNA**



TRANSLATIONS OF SELECTED PAPERS PUBLISHED IN  
NUCLEAR CONSTANTS 1(50) 1983  
(Russian original distributed as INDC(CCP)-213/G)

Translated by the IAEA

November 1984

Reproduced by the IAEA in Austria  
November 1984

84-06218

## Table of Contents

	<u>Page</u>
1. Investigation of the Mechanism of Fast Neutron Scattering by Even Isotopes of Molybdenum. By I.A. Korzh, V.P. Lunev, V.A. Mishchenko, Eh.N. Mozhzhukhin, N.M. Pravdivyj and E.Sh. Sukhovitskij.	1
2. Evaluation of Fast-Neutron Radiative Capture Cross-Sections for Samarium and Europium Odd Isotopes. By B.D. Yurlov, T.S. Belanova, A.V. Ignatyuk, V.N. Kononov and G.N. Manturov.	15
3. Covariance Matrix of Experimental Data on the Energy Dependence of $\bar{\nu}_p$ for Neutron-Induced Fission of the Nuclei $^{232}\text{Th}$ , $^{236}\text{U}$ , $^{238}\text{U}$ , $^{237}\text{Np}$ . By V.V. Malinovskij, B.D. Kuz'minov and V.G. Vorob'eva.	46



INVESTIGATION OF THE MECHANISM OF FAST NEUTRON SCATTERING  
BY EVEN ISOTOPES OF MOLYBDENUM

I.A. Korzh, V.P. Lunev, V.A. Mishchenko, Eh.N. Mozzhukhin,  
N.M. Pravdivyj and E.Sh. Sukhovitskij

ABSTRACT

Experimental differential and integral cross-sections of elastic and inelastic scattering of neutrons by the isotopes  $^{92}\text{Mo}$  and  $^{94}\text{Mo}$  are given. The experimental data are analysed in the framework of the spherical optical model, of the coupled-channel method and also of up-to-date versions of the statistical theory of nuclear reactions. A theoretical analysis is used to determine the ratio of the contributions of the two scattering mechanisms, namely direct scattering and scattering through a compound nucleus.

The widespread use of molybdenum in present-day and future nuclear and thermonuclear facilities is giving rise to requirements for systematic data of fairly high accuracy on the interaction cross-sections of neutrons with isotopes of this element. In addition, isotopes of molybdenum are among the most common fission fragments. From the physical point of view, the study of the dynamics of variations in the mechanism of neutron scattering by even isotopes of molybdenum with neutron energies varying within the region of a few MeV is of great interest since their different positions in respect of the magic number of 50 neutrons mean that they have very great differences in the energy structures of nuclear levels and types, which are manifested in different coefficients of quadrupole deformation.

Up to neutron energies of 4 MeV, the literature contains elastic scattering cross-sections [1-3] and inelastic scattering cross-sections with excitation of discrete levels of the nucleus  $^{92}\text{Mo}$  [3]. There is little information on neutron scattering cross-sections in the energy region above 4 MeV because of the experimental difficulties arising when obtaining them. In this energy region there are only the data of Ref. [4] on neutron elastic scattering cross-sections by the nucleus  $^{92}\text{Mo}$ . There are even fewer data on neutron elastic [1,2] and inelastic [1,2,5] scattering cross-sections by the nucleus  $^{94}\text{Mo}$ . New measurements of the neutron elastic and inelastic scattering cross-sections by these isotopes over a wide range of energies will thus be useful.

Measurements have been made of the differential neutron elastic and inelastic scattering cross-sections with excitation of the first levels of the nuclei  $^{92}\text{Mo}$  and  $^{94}\text{Mo}$  at initial neutron energies of 1.5, 2.0, 2.5, 3.0, 5.0, 6.0 and 7.0 MeV. The experimental differential cross-sections obtained have been analysed in accordance with the theory of the spherical optical and statistical model and also with the coupled-channel model. In order that the analysis in the context of the above-mentioned models should be sufficiently full, the energy dependences of the total and integral elastic and inelastic scattering cross-sections in the energy range 0.5-9.0 MeV measured in this study and of those found in the literature have also been analysed.



### Experimental method

The differential elastic and inelastic scattering cross-sections were measured on an EhG-5 pulsed electrostatic accelerator with a high-resolution time-of-flight fast-neutron spectrometer [6,7] adapted for measurements in the energy range 1.0-7.0 MeV. Neutrons with an energy spread of  $\pm$  (90-140) keV obtained in the  $T(p,n)^3\text{He}$  and  $D(d,n)^3\text{He}$  reactions with hard Ti-T and Ti-D targets were scattered by cylindrical samples made from pressed metal powders highly enriched in the corresponding isotope: 92.2% for  $^{92}\text{Mo}$  (mass 55 g) and 87.7% for  $^{94}\text{Mo}$  (mass 43.5 g). The samples were placed at a distance of 10 cm from the target.

The scattered neutrons were detected at drift distances of up to 3 m and at 9-15 different angles in the range 20-150° by a scintillation detector (a stilbene crystal with an FEhU-30 photoelectron multiplier) with an n- $\gamma$  separator placed in a solid protective collimator with an additional shadow shield. The neutron collimation system provides sufficiently good measurement conditions even with relatively low sample masses and average proton or deuteron currents to the target of 1-5  $\mu\text{A}$ .

The neutron flux was monitored with a long counter, a time-of-flight detector placed at an angle of 30° to the primary particle beam and a current integrator.

The neutron spectrometer and the measurement technique are described in detail in Refs [6,7].

### Measurement results

The scattered neutron spectrum measurements were used to determine the differential elastic scattering cross-sections by normalization to the neutron flux at an angle of 0° and the differential inelastic scattering cross-sections with excitation of the first levels of the molybdenum isotopes investigated by normalization to the well-known scattering cross-sections of neutrons by hydrogen in a polyethylene sample of small diameter (mass 1.3 g) at angles at which the neutrons scattered have the same energies as inelastically scattered neutrons with excitation of the corresponding levels of molybdenum isotopes.

An analytical method was used to make corrections to the differential elastic and inelastic scattering cross-section measurements for attenuation of the neutron flux in the sample and for anisotropy of neutron emission from the

sample and to the differential elastic scattering cross-sections for the angular resolution in the experiment and for multiple scattering of neutrons in the sample [8].

The differential elastic and inelastic scattering cross-sections of neutrons by the isotopes  $^{92}\text{Mo}$  and  $^{94}\text{Mo}$  obtained at the neutron energies investigated are shown in Figs 1a and b. The errors shown in Figs 1a and b are total errors and include errors of measurement, normalization and correction.

The differential elastic scattering cross-sections of neutrons by the nucleus  $^{92}\text{Mo}$  at low energies found by the authors agree well with those in the literature [2,3]; the remaining differential cross-sections are found for the first time.

By integration of the differential cross-sections we obtained integral elastic and inelastic scattering cross-sections for neutrons of the investigated energies using the isotopes  $^{92}\text{Mo}$  and  $^{94}\text{Mo}$ .

For purposes of comparison and analysis, Figs 2 and 3 show the energy dependences of total and integral neutron elastic and inelastic scattering cross-sections including the data of the present paper and published data of other authors. It will be seen from Figs 2 and 3 that the data in the literature generally correlate well with the results obtained by the authors of this paper.

#### Theoretical analysis of experimental data

Theoretical analysis of the experimental data was based on the optical-statistical approach combined with the coupled-channel method [10].

In order to calculate the total and differential potential elastic scattering cross-sections and also the transmission coefficients needed for calculating cross-sections with the statistical theory, use was made of the optical model of the nucleus with a spherical potential of the type

$$V(r) = -V_c f(r) - iW_c g(r) + V_{so} \left(\frac{\hbar}{m\pi c}\right)^2 \frac{1}{r} \frac{d}{dr} f(r) \vec{\sigma} \vec{l}, \text{ where } f(r) = \left[1 + \exp\left(\frac{r-R}{a}\right)\right]^{-1},$$

$$g(r) = \exp\left[-\left(\frac{r-R}{b}\right)^2\right], R = r_0 A^{1/3}, [11] \text{ and with the set of averaged potential parameters of Ref. [12]:}$$

$$\begin{aligned} V_c &= (48.7 - 0.33E) \text{ MeV}; W_c = (7.2 + 0.66E) \text{ MeV}; V_{so} = 7.5 \text{ MeV}; \\ a &= 0.65 \phi; b = 0.98 \phi; r_0 = 1.25 \phi. \end{aligned} \quad (1)$$

The direct inelastic scattering cross-sections were calculated by the coupled-channel method [13] in which the system of linked Schrödinger equations for the radial functions  $R_{Jn\ell j}(r)$  with fixed values of  $J$  and  $\Pi$  has the form

$$\left( \frac{d^2}{d\rho_n^2} - \frac{\ell_n(\ell_n-1)}{\rho_n^2} - \frac{V_{diag}}{E_n} + 1 \right) R_{Jn\ell_n j_n}(z) = \frac{1}{E_n} \sum_{n'\ell_n' j_n'} R_{Jn'\ell_n' j_n'}(z) \times \quad (2)$$

$$\times \langle (Y_{\ell_n j_n} \otimes \phi_{I_n})_{JM} | V_{couple} | (Y_{\ell_n' j_n'} \otimes \phi_{I_n'})_{JM} \rangle,$$

where  $\rho_n = k_n r$  ( $k_n$  is the wave number of a neutron of energy  $E_n$ );  $Y_{\ell j}$  is a spherical spin-angle function with orbital moment  $\ell$  and total moment of the neutron  $j$ ;  $\phi_{I_n}(\xi)$  is the wave eigenfunction of the Hamiltonian of a target nucleus with moment  $I_n$  and its  $z$ -projection  $M_n$ ; and  $\otimes$  is the vector addition of functions. The channel energy  $E_n$  is linked with the energy of the  $n$ -th state  $\epsilon_n$  by the relationship  $E_n = E - \epsilon_n$  ( $n = \text{unity minus the ground state of the target nucleus}$ ). The primes stand for the quantum characteristics of all the emission channels permitted by the laws of conservation.

The interaction potential  $V(r, \theta, \phi)$  is represented in the form  $V(r, \theta, \phi) = V_{diag} + V_{couple}$ , where  $V_{diag}$  is the spherical optical potential and  $V_{couple}$  is the non-diagonal part of the optical potential resulting in the link between the different reaction channels. Where  $V_{couple} = 0$ , the system of linked equations (2) changes into the usual Schrödinger optical-model equation.

From Eq. (2) it will be seen that with the coupled-channel method the problem is reduced to selection of the link potential and to calculation of the matrix elements in accordance with a specific model for approximating the structure of lower levels of the target nucleus. For spherical nuclei the vibrational model with dynamic deformation is usually taken.

In the coupled-channel method the radius of deformed components of the potential  $V_c$  and  $W_c$  (when calculating the link potential the spin-orbital term may be ignored) is taken to be in the form  $R = R_0 [1 + \sum_{\mu} \alpha_{\mu} Y_{2\mu}(\theta, \phi)]$ , where  $R_0 = r_0 A^{1/3}$  and  $\beta_2 = \langle 0 | \sum_{\mu} |\alpha_{\mu}|^2 | 0 \rangle$ . The parameter  $\beta_2$  determines the strength of the link. On the assumption that excited levels are vibrational, in the explicit form account is taken only of the link between the ground state and the first excited level. For the calculations, the averaged parameters of the optical model (1) are used (except for  $W_c$ , which is reduced by

20% in order to obtain the same value of  $\sigma_c$  as in the spherical optical model). The calculations were performed using the program given in Ref. [14]. The quadrupole deformation coefficients  $\beta_2$  were taken to be 0.116 for  $^{92}\text{Mo}$  and 0.169 for  $^{94}\text{Mo}$  [15].

The differential cross-sections for scattering through a compound nucleus were calculated in accordance with the statistical theory, account being taken of fluctuations in level widths [16] by the method described in Ref. [17] according to the formula

$$\begin{aligned} \sigma_{nn'}(E, E', \theta) = & \frac{\lambda^2}{4} \frac{1}{2(2l+1)} \sum_{\ell j} T_{\ell j}(E) \sum_J (2J+1)^2 \times \\ & \times \frac{\sum_{\ell' j'} T_{\ell' j'}(E') R_{\ell j \ell' j'}^{J \Pi}}{\sum_{\ell'' j''} \left[ \sum_{E''} T_{\ell'' j''}(E'') + \int_{E''_{\max}}^E T_{\ell'' j''}(E'') \rho(U, i'') dE'' \right]} \times \\ & \times \sum_{L \text{ even}} (-1)^{l-l'} Z(\ell' j' \ell j'; \frac{1}{2} L) Z(\ell j \ell j'; \frac{1}{2} L) W(J j' J j'; l' L) W(J j J j; l L) P_L(\cos \theta), \end{aligned} \quad (3)$$

where  $E$ ,  $E' = E - \epsilon_q$  and  $E'' = E - \epsilon_p$  are the kinetic energies of neutrons (incident, emitted through the particular channel, and emitted through all permitted channels respectively);  $\epsilon_q$  and  $\epsilon_p$  are the excitation energies of the target nucleus level being studied and of any such level which is permitted, respectively;  $E''_{\max}$  is the energy of a neutron emitted with excitation of the last level considered to be discrete;  $l$  and  $j$ ,  $l'$  and  $j'$  and  $l''$  and  $j''$  are the orbital and total angular momenta of neutrons (incident, emitted through the particular channel and emitted through all permitted channels respectively) permitted by conservation laws;  $J$  and  $\Pi$  are the spins and parities of the states of the compound nucleus;  $i$ ,  $i'$  and  $i''$  are the spins of the ground state, the excited state being studied, and all the permitted states of the compound nucleus, respectively;  $\lambda$  is the wavelength of the incident neutron;  $T_{\ell j}(E)$ ,  $T_{\ell' j'}(E')$  and  $T_{\ell'' j''}(E'')$  are the transmission coefficients for neutrons of the corresponding energies;  $R_{\ell j \ell' j'}^{J \Pi}$  is a coefficient taking into account the effect of level width fluctuations;  $Z$  are Blatt-Biedenharn coefficients;  $W$  are Racah coefficients;  $P_L$  are even Legendre polynomials; and  $\rho(U, i'')$  is the level density of the residual nucleus of a particular spin and both parities for an effective excitation energy  $U$ . In Eq. (3) the summation takes into account the conservation laws of total angular momentum and parity.

In the statistical-theory calculations, use is made of discrete levels of the molybdenum isotopes being studied which are taken from the compilation of Ref. [18]. Higher levels with unknown characteristics are treated statistically using the Fermi-gas model with "back bias". The level density in a solid spectrum was calculated with the formula of Ref. [19]

$$\rho(U, i'') = \frac{2i''+1}{24\sqrt{2} a^{1/4} U^{5/4} \sigma^3} \exp \left[ 2\sqrt{aU} - \frac{(i''+1/2)^2}{2\sigma^2} \right],$$

where  $U = E - \Delta$ ;  $a$  and  $\Delta$  are level density parameters; and  $\sigma$  is a spin cut-off parameter linked with  $a$ ,  $U$  and the nuclear mass  $A$  by the relationship  $\sigma^2 = 0.146 \sqrt{aU} A^{2/3}$  [20]. The values of the parameters  $a$  and  $\Delta$  were taken from Ref. [21] but renormalized for the use of a different expression for the level density.

The formula for the integral neutron inelastic scattering cross-section with excitation of a level of energy  $\epsilon_q$  in the Hauser-Feshbach-Moldauer (HFM) statistical theory has the form

$$\sigma_{nn'}(E, E') = \frac{\pi \lambda^2}{2(2i+1)} \sum_{l_j} T_{l_j}(E) \sum_J (2J+1) \frac{\sum_{l'_j} T_{l'_j}(E') R_{l'_j l_j}^{J\pi}}{\sum_{l''_j} \left[ \sum_{E''} T_{l''_j}(E'') + \int_{E''_{max}}^E T_{l''_j}(E'') \rho(U, l'') dE'' \right]} \quad (4)$$

If we assume  $R_{l_j l'_j}^{J\pi} = 1$ , the HFM formulae (3) and (4) turn into Hauser-Feshbach (HF) formulae, which do not take level width fluctuations into account.

Where only certain competing compound-nucleus decay channels are open, the coefficients  $R_{l_j l'_j}^{J\pi}$  for inelastic scattering become less than unity. With increasing energy, the coefficients  $R_{l_j l'_j}^{J\pi}$  tend to unity and the cross-sections calculated with the HFM and HF formulae coincide.

The HFM and HF formulae are valid if weak absorption in all channels ( $\Gamma \ll D$ ) is assumed. In recent years, formulae for calculating fluctuation cross-sections for strong absorption ( $\Gamma \gg D$ ) have been given in a number of papers [22-24]. For example, Tepel, Hofmann and Weidenmüller (THW) [22] have found approximated expressions for the fluctuation cross-section based on representation of the cross-section in factorized form and on the condition of unitarity of the S-matrix. The THW formula for the fluctuation cross-section has the form

$$\sigma_{nn'}(E, E') = \frac{\pi \lambda^2}{2(2l+1)} \sum_{\ell_j} V_{\ell_j}(E) \sum_J (2J+1) \frac{\sum_{\ell_j'} V_{\ell_j'}(E')}{\sum_{\ell_j''} \left[ \sum_{E''} V_{\ell_j''}(E'') + \int_{E''_{\max}}^E V_{\ell_j''}(E'') \rho(U, l'') dE'' \right]} \times \quad (5)$$

$$\times \left\{ 1 + \sigma_{nn'} [W_{\ell_j}(E) - 1] \right\},$$

where  $V_{\ell_j}$  and  $W_{\ell_j}$  are parameters which depend on the optical-model transmission coefficients in the following way

$$V_{\ell_j} = T_{\ell_j} \left[ 1 + (T_{\ell_j} / \sum_{\ell_j''} T_{\ell_j''}) (W_{\ell_j} - 1) \right]^{-1}; \quad (6)$$

$$W_{\ell_j} = 1 + 2(1 + T_{\ell_j}^{1/2})^{-1}.$$

The parameter  $W_{\ell_j}$  in Eq. (5) reflects the effect of correlation strengthening of the elastic scattering cross-section. The approximating expression (6) for  $W_{\ell_j}$  was obtained on the assumption that  $W_{\ell_j}$  is a function of only one channel  $T_{\ell_j}$ . Reference [23] gives a more exact expression for  $W_{\ell_j}$  including not only the dependence on the transmission coefficient for the particular channel but also the slight dependence on the transmissions for other channels.

As was to be expected, the results of calculations using the THW formula lie between the predictions of the HF and HFM formulae. With an increase in neutron energy - and therefore in the number of open channels - cross-sections calculated with HFM and THW become more and more similar and at neutron energies of a few MeV they practically coincide. This makes it possible to use the more convenient THW formulae in calculations, since it ceases to be necessary to calculate the somewhat complex integrals contained in the fluctuation factor of the HFM formula.

In calculations of neutron scattering cross-sections for the nuclei being studied using the statistical theory with the help of the normalization factor  $(\sigma_a - \sigma_{np} - \sigma_{n\alpha}) / \sigma_a$  account has been taken of competing channels with emission of protons and  $\alpha$ -particles [25], since in the calculation formulae only neutron emission channels were considered.

In Figs 1-3 the results of calculations using the models discussed above are shown for purposes of comparison with experimental data. The differential and integral neutron elastic scattering cross-sections are shown as the sums of the cross-sections calculated with the spherical optical model and with the

HFM statistical theory. Figure 4 shows differential neutron elastic scattering cross-sections through a compound nucleus for  $^{92}\text{Mo}$  and  $^{94}\text{Mo}$  at  $E_n = 0.5-5.0$  MeV calculated with the HFM theory. The neutron inelastic scattering cross-sections through the compound nucleus are added to the direct inelastic scattering cross-sections in accordance with the formula  $\sigma_{nn'}^T = ((\sigma_a - \sigma_{nn'}^D)/\sigma_a)\sigma_{nn'}^{\text{CN}} + \sigma_{nn'}^{\text{DN}}$ , where  $\sigma_{nn'}^{\text{CN}}$  is the cross-section of inelastic scattering through a compound nucleus;  $\sigma_{nn'}^D$  is the direct inelastic scattering cross-section calculated with the coupled-channel method; and  $\sigma_a$  is the absorption cross-section.

From Figs 1-3 it will be seen that the total cross-sections for the isotopes considered which are calculated with the spherical optical model agree well with experimental data, while the differential and integral neutron elastic and inelastic scattering cross-sections calculated with the HFM or THW statistical theory and the spherical optical model or with the coupled-channel method agree well enough with experimental data within the energy range covered for conclusions to be drawn about the role of direct and compound processes with neutron scattering. Thus, direct (potential) neutron elastic scattering at the beginning of the energy range studied is in these calculations approximately 50% of the total, while at the end of the range it begins to predominate. At the beginning of the energy range studied, direct inelastic scattering cross-sections with excitation of the first  $2^+$  levels do not exceed 15% of the total for the molybdenum isotopes examined, while at the end of the range they also begin to predominate.

The analysis performed not only makes it possible to draw conclusions about the roles of the various mechanisms in fast neutron scattering, but also indicates the possibility of using the theoretical models applied for predicting the fast-neutron scattering cross-sections for isotopes of molybdenum.

#### REFERENCES

- [1-4, 8, 9, 11, 13, 15, 16, 18-25] [See original]
- [5] KONOBEVSKIY, E.S., MUSAELIAN, R.M., POPOV, V.I., SURKOVA, I.V., *Fiz. Ehlem. Chastits At. Yadra* 13 (2) (1982) 300.
- [6] ZHUK, V.V., KOZAR', A.A., KORZH, I.A., in: *Nejtronnaya fizika (Neutron Physics)*, (Proc. II All-Union Conf. on Neutron Physics, Kiev, 28 May-1 June 1973), 4 Obninsk (1974) 203.

- [7] KORZH, I.A., MISHCHENKO, V.A., SANZHUR, I.E., Ukr. Fiz. Zh. 25 (1) (1980) 109.
- [10] KORZH, I.A., MISHCHENKO, V.A., MOZHZHUKHIN, Eh.N. et al., Yad. Fiz. 31 (1980) 13.
- [12] PASECHNIK, M.V., KORZH, I.A., KASHUBA, I.E., in: Nejtronnaya fizika (Neutron Physics), 1 Kiev, Naukova dumka (1972) 253.
- [14] IGNATYUK, A.V., LUNEV, V.P., SHORIN, V.S., Voprosy atomnoj nauki i tekhniki, Ser. Yadernye konstanty 13 (1974) 59.
- [17] KORZH, I.A., KASHUBA, I.E., GOLUBOVA, A.A., in: Nejtronnaya fizika (Neutron Physics), (Proc. III All-Union Conf. on Neutron Physics, Kiev, 9-13 June 1975) 4 TsNIIatominform, Moscow, (1976) 203; ANTSIPOV, G.V. et al., Voprosy atomnoj nauki i tekhniki, Ser. Yadernye konstanty 20 (1975) 164.

Paper received by Editors on 5 January 1983.



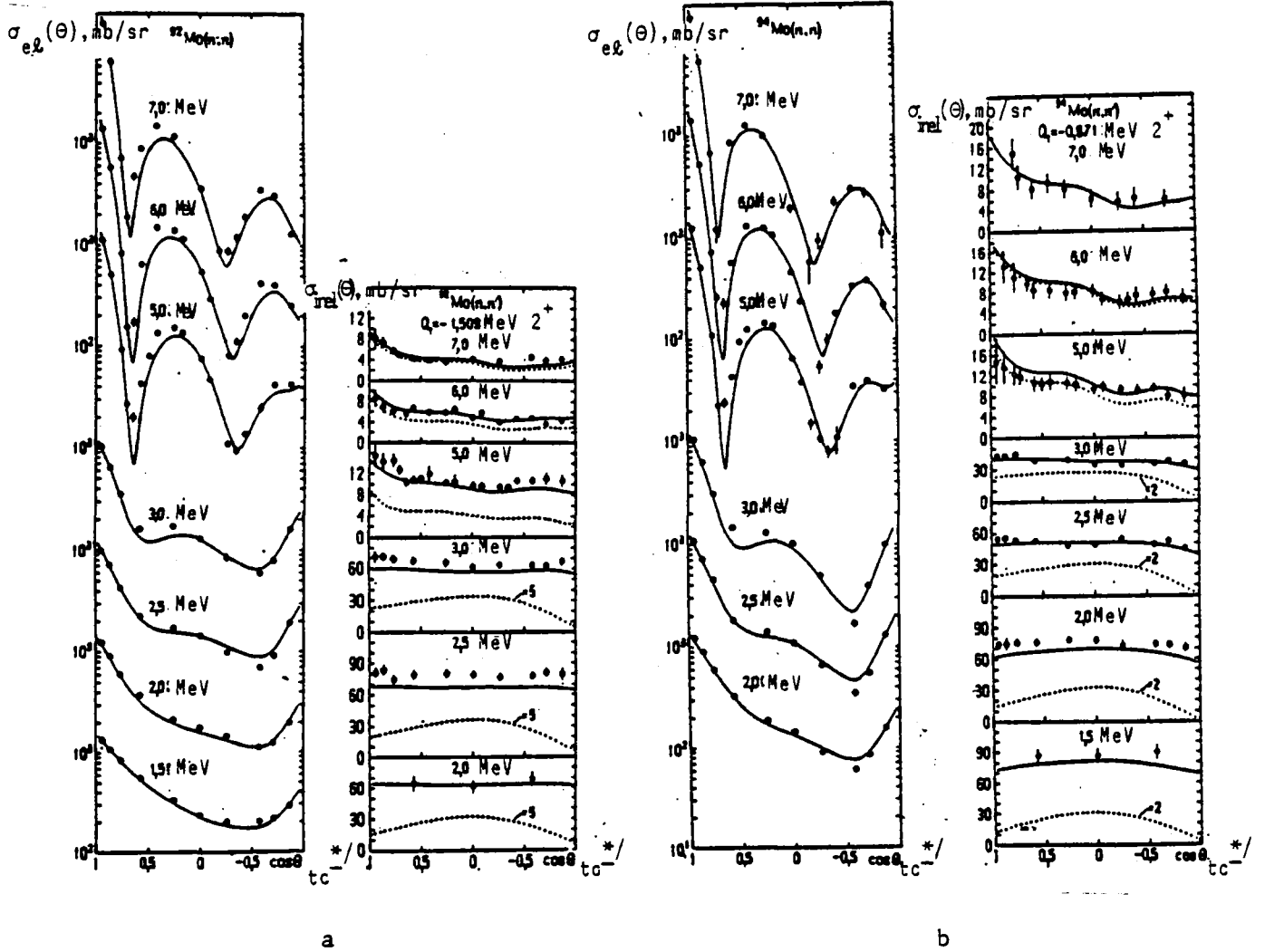


**Fig. 1.** Differential neutron elastic and inelastic scattering cross-sections at energies of 1.5–7.0 MeV for the nuclei  $^{92}\text{Mo}$  (a) and  $^{94}\text{Mo}$  (b). The experimental data of this paper are shown as circles; the solid lines stand for elastic scattering calculated with the spherical optical model and the HFM statistical theory and for inelastic scattering calculated with the coupled-channel method and the HFM statistical theory; and the dotted lines show calculations with the coupled-channel method.

\* /  $tc = \text{centre of mass.}$

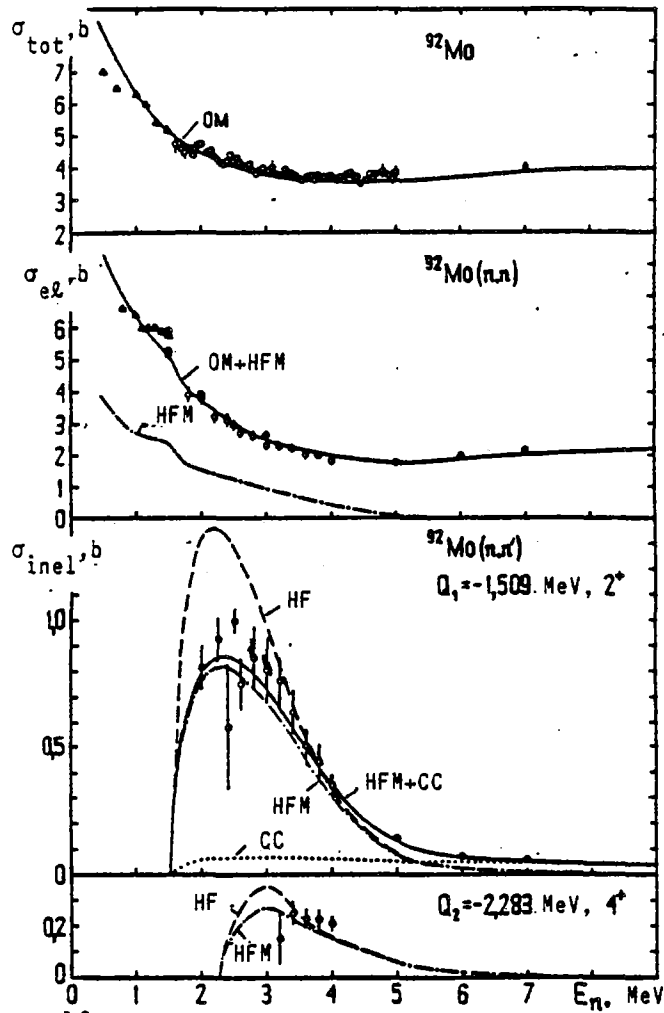


**Fig. 2.** Energy dependences of total and integral neutron elastic and inelastic scattering cross-sections with excitation of the first two levels of the  $^{92}\text{Mo}$  nucleus in the energy region 0.5-9.0 MeV. Experimental cross-sections:  $\bullet$  = this paper;  $\Delta$  = Ref. [1];  $\square$  = Ref. [2];  $\circ$  = Ref. [3]; and  $\diamond$  = Ref. [9]. Theoretical calculations: OM = spherical optical model; CC = coupled-channel method; HF = statistical model without considering fluctuations in level widths; and HFM = statistical model with level width fluctuations considered.

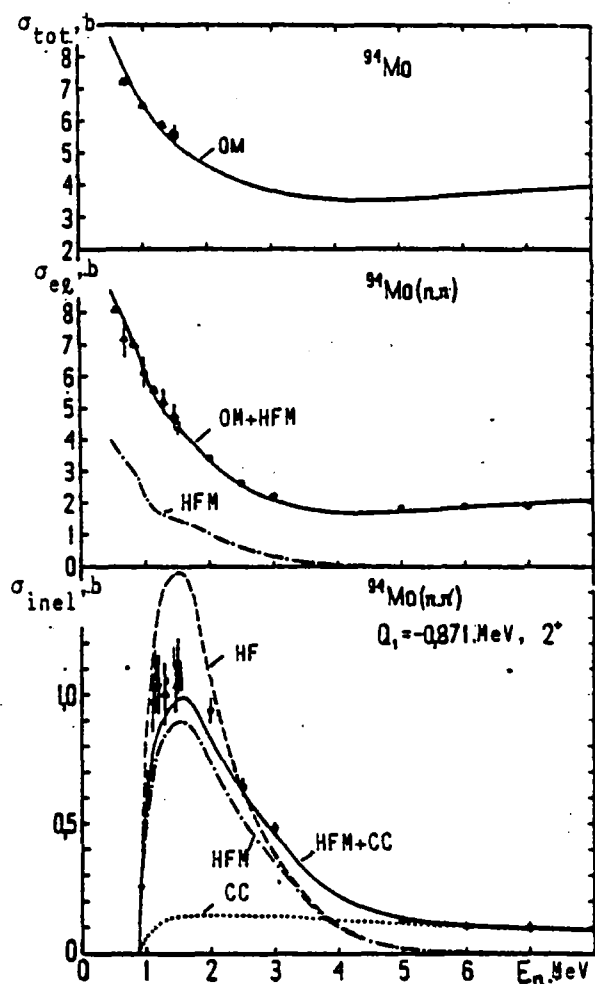


**Fig. 3.** Energy dependence of total and integral neutron elastic and inelastic scattering cross-sections with excitation of the first two levels of the  $^{94}\text{Mo}$  nucleus in the energy region 0.5-9.0 MeV. Experimental cross-sections:  $\bullet$  = this paper;  $\Delta$  = Ref. [1];  $\square$  = Ref. [2]; and  $\blacktriangledown$  = Ref. [5].

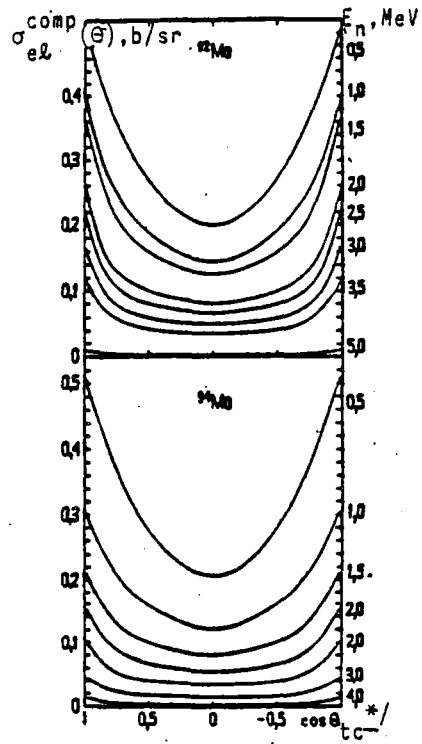


Fig. 4. Differential neutron elastic scattering cross-sections through the  $^{92}\text{Mo}$  and  $^{94}\text{Mo}$  compound nucleus at  $E_n = 0.5-5.0$  MeV as calculated by the statistical theory with level width fluctuations considered.

\*/  $t_c =$  centre of mass.

UDC 539.172.4/173.4

EVALUATION OF FAST-NEUTRON RADIATIVE CAPTURE CROSS-SECTIONS  
FOR SAMARIUM AND EUROPIUM ODD ISOTOPES

B.D. Yurlov, T.S. Belanova, A.V. Ignatyuk,  
V.N. Kononov and G.N. Manturov

The process of nuclear fuel burnup in the reactor core results in the accumulation of an appreciable quantity of fission products, which are liable to have considerable effect on the neutron balance in the reactor. Consequently, many problems relating to core poisoning arise in the course of designing and operating nuclear reactors. To overcome them it is necessary to have accurate information on the neutron cross-sections of fission products and, in particular, the neutron radiative capture cross-sections. To this end a large number of evaluations of fission product cross-sections have been published, the most complete being the compilations [1-5]. According to the evaluations conducted, an accuracy of 15-20% is attained for the fast-neutron radiative cross-sections of fission products. However, in order to obtain an error of 1% when calculating  $K_{eff}$  and 2% in the value of the breeding ratio of a fast reactor operated on plutonium oxide fuel with sodium coolant, approximately twice that degree of accuracy [6,7] is required. As shown in Ref. [8], the uncertainty in  $K_{eff}$  is at present almost entirely a function of the neutron cross-section errors already determined for fission products.

Odd isotopes of samarium are among the first ten or so most important fission products responsible for reactor core poisoning. The odd isotopes of europium, however, have great potential as a material for reactor control rods. Since there is considerable spread of the data in the evaluations of neutron capture cross-sections for both elements [1-5], the task of analysing the reasons for it and reducing the error of the evaluated values is one of topical relevance. This, in fact, is the task the authors have set themselves in the present paper.

The status of the experimental data on fast-neutron radiative capture cross-sections

Table 1 sets out details of Refs [9-18], in which measurements are made of neutron radiative capture cross-sections for samarium and europium odd isotopes. Figures 1-6 show the energy dependence of capture cross-sections

for separated isotopes, while Figs 7 and 8 show the same dependence for a natural isotope mixture of these elements. Most of the experiments relating to the neutron energy region 1-1000 keV use a method which involves recording the prompt  $\gamma$ -radiation for capture and applying the time-of-flight or slowing-down time technique in order to determine neutron energy. This method is used in experiments involving a lead slowing-down time spectrometer (STD or "lead cube") [11,19] and linear-accelerator [13-15,17,18] and electrostatic-accelerator spectrometers [10,16,20,21]. The neutron radiative capture events were recorded chiefly by means of total-energy detectors or large scintillation tanks. Neutron flux was measured from the reactions  $^{10}\text{B}(n,\alpha\gamma)^7\text{Li}$  and  $^6\text{Li}(n,\alpha)\text{T}$ . These methods are described in greater detail in a number of published papers such as Ref. [22].

Using the lead cube, which has a comparatively high neutron flux density, it is possible to measure low cross-section values. In the region of tens of keV, however, its energy resolution is poor (around 60-100%).

One merit of spectrometers based on linear electron accelerators (LEA) is that they permit the study of a wide range of neutron energies (from resonance to fast neutrons), so that the value of  $\sigma_c$  can be absolutized by the saturated resonance method. They also have disadvantages, however, one of which is the existence of a background - dependent on flight time - in the region above 10-20 keV, its source being fast scattered neutrons. This background is responsible for the low accuracy in this energy region of the measurement of  $\sigma_c$  by means of the LEA, it being difficult to determine the variable background unambiguously.

The advantage of electrostatic-accelerator spectrometers is that they produce a low neutron background which can be calculated accurately if measured simultaneously with the capture effect. The disadvantage of such spectrometers lies in the low ratio between the latter effect and background in the 1-10 keV energy region, due to the relatively low neutron yield from the  $^7\text{Li}(p,n)^7\text{Be}$  reaction, which has the effect of appreciably increasing the  $\sigma_c$  error in this energy range.

It should be noted that, as a result of the systematic research on samarium and europium isotopes conducted in recent years, we now have far more information on the  $\sigma_c(E)$  value for these nuclei than previously, although the results of individual studies (see Fig. 1) show significant discrepancies - greater than the errors indicated by the authors - for both energy dependence and the absolute cross-section values.

$^{147,149}\text{Sm}$ . For  $^{147}\text{Sm}$  in the energy region 5-300 keV there are two sets of data for the value  $\sigma_c(E)$  [16-18] which differ in slope and do not intersect anywhere within the limits of the indicated experimental errors (see Fig. 1); below 10 keV the value of  $\sigma_c(E)$  determined by Kononov et al. [16] is approximately twice as high as that determined by the Japanese group [18], this difference decreasing to 25-30% at 200-300 keV. It may be noted that in Ref. [18]  $\sigma_c(E)$  passes through Macklin's point [10] at 30 keV.

The values of  $\sigma_c(E)$  established for  $^{149}\text{Sm}$  are given in Refs [14,16,18]. Above 10-15 keV they are in good agreement (see Fig. 2), but below this energy the capture cross-section obtained by Kononov et al. [16] has a steeper  $\sigma_c(E)$  curve. Macklin's single point at 30 keV is approximately 60% below all the other results.

$^{151,153}\text{Eu}$ . References [11,13-17] give data for  $\sigma_c(E)^{151}\text{Eu}$  which agree with an average of 10% accuracy up to 60 keV. In the energy region 60-100 keV two sets of data may be distinguished:  $\sigma_c(E)$  from Refs [14,16], which agree within limits of 4-7% but are consistently about 25% lower; and  $\sigma_c(E)$  from Refs [15,17], which agree within limits of 2-11%.

No data are available for the higher neutron energy in Refs [15,17], but the  $\sigma_c(E)$  curve from Ref. [14] rises 10-35% higher than that obtained in Ref. [16]. The activation cross-sections obtained by Johnsrud [9] by means of the "two-ratio" method proved to be two to three times lower than the other values of  $\sigma_c(E)$  [14,16]. Renormalization of the Ref. [9] data to the recommended thermal capture cross-section for  $^{151}\text{Eu}$  [27] eliminates this disagreement.

The experimental data for the cross-section of  $^{153}\text{Eu}$  [13-17] also fall into two groups showing a marked difference in respect of the slope of the  $\sigma_c(E)$  curves (see Fig. 5), although as regards absolute values within the energy range 10-100 keV the different sets of data agree within limits of 20-15%. Between 160 and 300 keV Hockenbury's data [14] for this isotope - unlike  $^{151}\text{Eu}$  - are approximately 10% lower than those obtained in Ref. [16].

$^{151}\text{Sm}$ ,  $^{155}\text{Eu}$ . These nuclei are radioactive fission products, for whose fast-neutron capture cross-sections no experimental data are available.

$^{62}\text{Sm}$ ,  $^{63}\text{Eu}$ . There are few data on the natural isotope mixtures of these elements. Apart from the aforementioned studies, we have the data obtained by Chou [19] using a lead cube and also the measurements performed by Lepine [20], Macklin [21,23], Block [24] and Poenitz [25]. The cross-sections for natural samarium (see Fig. 7) obtained in Refs [19,24], which agree with each other, are consistently about 30-40% lower than those obtained by Kononov et al. [16]. The data of Refs [20,21,24] agree with the latter within the limits of the experimental measurement errors. For natural uranium (see Fig. 8) the situation regarding experimental data is much the same as for its separated isotopes. Within the range 15-70 keV most of the data intersect. Below 15 keV the  $\sigma_c(E)$  curves obtained in Refs [13,14,24] give values 15-25% higher than those obtained in Refs [11;15,17,19,20], while in the region 70-300 keV, on the other hand, the data from Refs [16,21] are 20-40% lower than those adduced in Refs [15,17,20].

Examination of the experimental data as a whole revealed a number of common features. Between approximately 10-15 and 70-80 keV the different sets of data agree by and large within experimental error limits. Below 10-15 keV the cross-sections obtained from electrostatic-accelerator spectrometers are normally higher (see, for example, the data given in Ref. [16]). In the region of hundreds of keV the data of Refs [14,15,17,18] exceed the corresponding data obtained on an LEA. The results obtained on an SDT [11,19] are almost invariably lower than in other studies. This obviously has something to do with the experimental methods used. As we have already mentioned, the low-energy region is difficult to measure by means of electrostatic accelerators. However, increasing neutron energy to hundreds of keV in resonance spectrometers has the effect of sharply increasing the scattered fast-neutron background, which makes it rather difficult to calculate the variable background correctly, hence the low accuracy and reliability of the data obtained. At a neutron energy of, for example, 100 keV, the data of Refs [14,15,17,18] have an error of 10-15%. Using the lead cube the energy resolution obtained in the energy region 15-50 keV is 60-100%, which complicates the interpretation and comparison of the experimental data and restricts the energy fields for the cross-sections used to 15-20 keV. Moreover, the procedure used in Refs [11,19] for absolutizing the capture cross-sections in terms of isolated resonance parameters or the neutron energy thermal region depends largely on calculation of the impurities from other isotopes [15,26] and on the resonance parameters used for normalizing the values obtained. In the examination of the data adduced in Refs [11,19] account should be taken of the following: firstly, the authors of Ref. [11]



state that the results obtained from different detectors (i.e. from proportional counters and scintillation detectors) differ by 20% and, secondly, the authors of Ref. [28] assert that the correction method used in Refs [11,19] with respect to multiple neutron scattering in the sample and resonance blocking is inaccurate and may result in a 10-20% reduction in the radiative capture cross-sections. The results of various relative measurements need to be renormalized to the most recent value obtained for the reference cross-sections. This applies in particular to the data of Lepine [20] and Macklin and Gibbons [21,23] for the capture cross-section of indium, for which this value is 10-15% higher than the one given in Ref. [29].

It should also be pointed out that consistency in the results of capture cross-section measurements for samarium, europium and their isotopes is found only in Ref. [16]. By "consistency" we mean that the value of  $\sigma_c(E)$  for natural isotope mixtures calculated from the experimental data for individual isotopes is in good agreement with the cross-section of natural  $^{62}\text{Sm}$  and  $^{63}\text{Eu}$  measured experimentally in the aforementioned study. This finding also applies to Ref. [17] for europium and its isotopes within an energy range of 3-100 keV. The consistency condition is not fulfilled, however, in Refs [10,18] for samarium and its isotopes or in Refs [11,14,15] for europium and its isotopes.

On the basis of the review made of the experimental situation and with a view to continuing the analysis, in order to obtain mean resonance parameters giving a satisfactory description of these experimental data we used the following studies: Refs [14,16,18] for  $^{147,149}\text{Sm}$  and  $^{151,153}\text{Eu}$ ; and [13,15] for  $^{151,153}\text{Eu}$ .

#### Evaluation procedure adopted

The evaluation of neutron cross-sections in the region of unresolved resonances is normally based on calculations following the optical model and statistical theory and involving data for the mean resonance parameters, i.e. the neutron  $S_0$  and radiative  $S_{\gamma 0}$  strength function values, data on the potential scattering radius  $R'$ , the level density parameter "a", the level scheme of the nucleus under investigation and other data obtained either experimentally or from the systematics derived from an analysis of the existing experimental information in conjunction with specific theoretical notions.

This generally accepted evaluation procedure is adopted in the present study, but in contrast to Refs [1-5], the values of  $S_\ell$  and  $S_{\gamma\ell}$  were determined on the basis of the aggregate analysis of the data obtained in the regions of isolated and unresolved resonances, respectively. Strength functions are derived from averaged radiative capture cross-sections by systematically comparing the experimental cross-section values with the theoretical capture cross-section curve calculated by means of the well-known Hauser-Feshbach-Moldauer equation [30]:

$$\sigma_c(E) = 2\pi^2 \lambda^2 \sum_{\ell I} g^J T_f^{\ell I} T_n^{\ell I} F \left( \frac{T_f^{\ell I}}{T_n^{\ell I}}, \frac{T_{in}^{\ell' I}}{T_n^{\ell I}} \right) / (T_f^{\ell I} + T_n^{\ell I} + T_{in}^{\ell' I}). \quad (1)$$

The penetrability factors  $T_n^{\ell I}$ ,  $T_{in}^{\ell' I}$  and  $T_f^{\ell I}$  are related to the adduced neutron  $S_\ell$  and radiative  $S_{\gamma\ell}$  strength functions as follows:

$$T_n^{\ell I} = \varepsilon_{\ell\ell I}^0 S_\ell v_\ell \sqrt{E} \left(1 + \frac{\pi}{2} S_\ell v_\ell \sqrt{E}\right)^{-2}; \quad T_{in}^{\ell' I} = \sum_k \varepsilon_{\ell\ell' I}^k T_n^{\ell' I}; \quad T_f^{\ell I} = g^I S_{\gamma\ell} \xi(E). \quad (2)$$

In expressions (1) and (2) the conventional notations are used. The function  $\xi(E)$  includes the energy dependence of the full radiative width, while the factor  $F$  denotes the fluctuation of neutron widths in elastic and inelastic neutron scattering channels. The penetrability coefficients  $v_\ell$  were calculated for a channel radius  $R = 1.3 \cdot A^{1/3}$ . The fluctuation factor  $F$  was derived from the closest approximation of the Porter-Thomas neutron width distribution [31].

When calculating the cross-sections we took into account the contributions of neutron waves with an orbital momentum  $\ell$  equal to 0,1,2,3 (the f-wave parameters were taken as being equal to the corresponding p-wave parameters). It was assumed that the adduced neutron strength function  $S_\ell$  was not dependent on the full spin of the state  $J$  and the radiative strength  $S_{\gamma\ell}$  function was taken as the ratio of the full mean radiative width to the mean distance between levels, i.e.  $S_{\gamma\ell} = \bar{\Gamma}_{\gamma\ell} / (2\ell+1)\bar{D}_\ell$  and for  $\ell = 0$ ,  $S_{\gamma 0} = \bar{\Gamma}_\gamma / \bar{D}_{\text{obs}}$ . The function  $\xi(E)$  was calculated on the assumptions of dipole radiation and the Lawrence dependence of the averaged transit matrix element, using a nuclear level density derived from the Fermi-gas model with allowance for collective effects [32].

In view of the fact that the averaged cross-sections contain a contribution by a large number of neutron resonances - not only of zero orbital momentum - it can be expected that in such an analysis the statistical fluctuations in neutron widths and distances between resonances will not limit the accuracy of the mean resonance parameters obtained and that we can determine the parameters for neutrons with a high orbital momentum ( $l$  equal to 1 and 2) more reliably than in the resonance region.

The best evaluation of the vector  $\vec{P}$  of the neutron and radiative strength functions, i.e. the evaluation giving the most satisfactory description of the experimental data, was obtained by means of the method of maximum probability by minimizing the quadratic equation  $S^2(\vec{P}) = [\vec{\sigma}_{\text{exp}} - \vec{\sigma}_{\text{theor}}(\vec{P})]^T V^{-1} [\vec{\sigma}_{\text{exp}} - \vec{\sigma}_{\text{theor}}(\vec{P})] + [\vec{P}_0 - \vec{P}]^T W_0^{-1} [\vec{P}_0 - \vec{P}]$ , where  $\vec{\sigma}_{\text{exp}}$  is the experimental and  $\vec{\sigma}_{\text{theor}}$  the theoretical neutron radiative capture cross-section derived from Eq. (1);  $V$  is the covariational error matrix of the experimental cross-section data; and  $\vec{P}_0$  and  $W_0$  are the a priori values of the mean resonance parameters and their covariational error matrix, which is assumed to be diagonal. If we adopt this approach, the covariational error matrix  $W$  of the optimum values of the  $\vec{P}$  parameters is calculated as follows:  $W = [H^T V^{-1} H + W_0^{-1}]^{-1} \times \max \{1\sigma^2\}$ , where  $H$  is the coefficient matrix of the cross-section sensitivity to the parameters;  $\sigma^2 = S^2(\vec{P})/N$  is the evaluation of dispersion corresponding to the  $\chi^2$ -distribution; and  $N$  is the number of experimental points. The diagonal elements of the  $W$  matrix determine the dispersion of the parameters, while the non-diagonal elements correspond to the covariational properties of the parameters obtained by means of the maximum probability method.

This method was carried out by means of the computer program EVPAR, using the high speed for BEhSM-6 computer (the ORPA program was used for the M 222 computer [33]), which enabled the experimental data for the full cross-section, the capture cross-sections and elastic and inelastic scattering to be described by means of the Hauser-Feshbach-Moldauer model. Optimum parameters could be sought for various variants with respect to the unknown parameters  $S_l$  and  $S_{\gamma l}$ . In particular, since the value of the neutron strength function for s-neutrons was known with fair certainty from the analysis of isolated resonances, the parameter  $S_0$  was usually fixed. The parameter  $S_{\gamma l}$  was determined on the assumption that the radiative strength function was independent of the orbital momentum of the incident neutron.

### Selection of parameters and discussion of the evaluated cross-sections

Table 2 sets out the parameters calculated from the evaluation in Refs [1-5] for the samarium and europium isotopes under study together with the results obtained by the authors of the present study.

#### Neutron strength functions

The experimental data on neutron strength functions were analysed in Refs [27,34-37]. For the majority of nuclei the value of  $S_0$  is known from measurements in the resolved resonance region and for 20 of the most important fission products  $S_0$  is determined with an accuracy of  $\pm 30\%$  (or as good as  $\pm 10\%$  under certain favourable conditions). The dependence of  $S_0$  on mass number  $A$ , equal to 140-180, is shown in Fig. 9, which gives the experimental points and theoretical curves. The calculations based on the collective model and the coupled-channel method clearly give a more satisfactory description of the experimental data. The experimental values of  $S_0$  given in the collection of resonance parameters [27] and Refs [38,39] are taken as the recommended values of  $S_0$ .

The experimental data on  $S_1$  (Fig. 10) are less detailed and refer mainly to region A, where  $A$  equals approximately 100, and the rare-earth region. It should be noted that the values of the p-wave neutron strength function differ widely in many cases and are not very accurate or reliable. For the d-wave neutron strength function the only data available are the individual results obtained from an analysis of mean cross-sections (Fig. 11). Various forms of the collective model calculations [36,37,40] give an acceptable but as yet purely qualitative description of the entire set of experimental data on  $S_1$  and  $S_2$  as a function of atomic number.

For  $^{147,149}\text{Sm}$  and  $^{151,153}\text{Eu}$  the values of the strength functions for p- and d-neutrons are given in Ref. [17], where they serve as a basis for the process of matching. For the radioactive isotopes  $^{151}\text{Sm}$  and  $^{155}\text{Eu}$ , the values of  $S_1$  and  $S_2$  were selected on the basis of the observed experimental and theoretical trend of the dependence  $S_\lambda = 1.2(A)^\lambda$ . The a priori and recommended evaluations of the other parameters ( $S_{\gamma\lambda}$ , "a") were selected in a similar way.

Radiative strength functions. Level density parameter "a"

The values of  $S_{\gamma\ell}$  ( $\ell = 0,1,2$ ) are determined for many rare-earth nuclei in Refs [16,37]. It is also found that  $S_{\gamma 0}$  is often greater than the radiative strength function obtained by analysing isolated s-resonances, while the values of  $S_{\gamma\ell}$  obtained independently for s-, p- and d-neutrons are essentially dissimilar. The values of  $S_{\gamma} = S_{\gamma 0}$  from Refs [16,37] were used as initial values for the cross-section analysis.

Taking account of collective effects, values were selected at  $m^2 = 0.24 A^{2/3}$  [32] from Ref. [37] (Fig. 12) as recommended values for the level density parameter "a". Allowing for collective effects results in an appreciable decrease - virtually 5-10 reciprocal MeV - in the value of parameter "a" for rare-earth elements.

A discrete level scheme was formulated in accordance with Ref. [2] to take account of the competition of the capture reaction with inelastic scattering.

In the investigated neutron energy region of 1-1000 keV the sensitivity of the radiative capture cross-section to the various parameters of the calculation model varies. In particular, at  $E_n = 1-50$  keV  $\sigma_c$  is determined by the value of  $S_0$  and  $S_{\gamma 0}$ . At higher energies the p- and d-waves begin to play a tangible role and at  $E_n = 1$  MeV their contribution is crucial. Moreover,  $\sigma_c$  is affected by the adopted energy dependence  $\bar{D}$ ,  $\bar{\Gamma}_{\gamma}$  of the level density parameters. In the present study the influence of the calculation model parameters on the extent and nature of cross-section behaviour was examined. It emerged that calculation at the resonance value  $S_{\gamma}$  adduced in Ref. [27] for odd samarium and europium isotopes did not satisfactorily describe the experimental data: the calculated curve was located significantly lower - two to three times lower, in fact - than the experimental curve. In order to eliminate this discrepancy it is necessary sharply to increase either the value of  $S_0$  (to  $(8-10) \cdot 10^{-4}$ ) or the radiative strength function. Such high values of the s-wave neutron strength function yield manifestly exaggerated results for the cross-section at energies below 10 keV, a situation which conflicts with the experimental data. A fairly satisfactory description is obtained by increasing  $S_1$  to  $(3-6) \cdot 10^{-4}$ , but here the calculated cross-section has a considerably flatter energy curve, while at  $E_n = 1$  MeV correspondingly higher cross-section values are obtained. Furthermore, such values of  $S_1$  do not agree with those predicted by the optical model, which in the region of atomic weights  $A = 140-160$  yields a minimum dependence

of  $S_1$  on  $A$ . Consequently, in virtually all the known evaluations aimed at fitting the theoretical curve to the experimental data we have to step up the values of the radiative strength function  $S_\gamma$ . The influence of the level density parameter "a", its values and the nature of the model (whether or not it takes account of collective disturbances) is insignificant as regards the investigated nuclei and energy range 1-1000 keV. For example, at  $E_n = 1$  MeV inclusion of collective disturbances in the calculation of level density results in a 10-15% decrease in the cross-section, which is considerably less in principle than the effect at this energy of parameters such as the d-wave neutron strength function, the level scheme adopted and the model allowing for the fluctuations of mean resonance parameters. The results of the calculations and an analysis for each nucleus investigated are set out below.

$^{147}\text{Sm}$ . The curve calculated on the basis of the parameters recommended by the authors of the present study, which at  $S_\gamma$ , however, is equal to the resonance value from Ref. [27], is represented by the dotted line in Fig. 1. The description of the data of Ref. [18] using the method of maximum probability gives the following values:  $S_1 = 0.14 \pm 0.04$ ;  $S_2 = 1.7 \pm 0.44$ ;  $S_\gamma = 210 \pm 4^{*/}$ ; the calculated curve is close to the evaluation JENDL-1. Kononov's data [16] are described well by the parameters obtained in the present study. The description of the results of Refs [16,18] provides the recommended parameters set out in Table 2, while the theoretical curve derived from them is represented by a solid line in Fig. 1. The recommended curve rises higher than in a number of other evaluations [1,2,4,5], including, in particular, that of JENDL-1 (see Figs 1-6). This is because the value of  $S_\gamma$  obtained is greater than in Refs [1-5] and agrees with Gruppelaar's evaluation [3]. At a neutron energy of 30 keV various evaluations (see Table 2) agree to within 40%; at  $E_n = 1000$  keV the evaluations differ by a factor of over 2.

For the isotope  $^{149}\text{Sm}$  there are significantly more experimental data available than for  $^{147}\text{Sm}$ . The method of maximum probability therefore lends itself to a description of them. The process of matching the theoretical curve to three sets of experimental data simultaneously [14,16,18] results in optimum parameters, which are the recommended ones, while that of describing the experimental data of the aforementioned authors individually yields parameters which

---

\*/ Strength functions are expressed here and later in units of  $10^{-4}$ .

agree with the recommended parameters within error limits. The calculated curve based on resonance parameters and represented by a dotted line in Fig. 2 lies below the experimental points. As regards comparison with other evaluations, the adopted calculated curve at  $E_n = 30$  keV is 25% higher than the RCN-2 evaluation [3] and approximately 40% higher than the other evaluations [1,2,4,5]; at  $E_n = 1000$  keV various evaluations once again differ by a factor of 2 or more. The discrepancy at a neutron energy of 30 keV is primarily due to the fact that the other evaluations [1,2] are normalized at this energy to the neutron radiative capture cross-section for  $^{149}\text{Sm}$  obtained in Ref. [10], whose value is 1.6 times lower than that of the other data [14, 16,18]. The discrepancy in the theoretical cross-sections at high neutron energies may be due to a number of different factors, including, for example, the different level scheme or calculation models used.

There are no experimental data for  $^{151}\text{Sm}$ , which is why Fig. 3 gives theoretical curves only (the evaluation made in the present study together with JENDL-1) [2]. The authors of Ref. [2] used the resonance value of the radiative strength function ( $S_\gamma = 500$ ), which is accordingly located below the recommended curve, although for the neighbouring samarium isotopes ( $^{147,149}\text{Sm}$ ) the same authors increase this parameter by a factor of almost 2 above its resonance value. The value of  $S_\gamma$ , equal to 1200, is taken from the systematics for  $S_\gamma(A)$  with respect to the neighbouring nuclei [16,37] (in the same way, incidentally, as other essential parameters). The parametric errors are also evaluated on the basis of the uncertainty of such parameters for neighbouring isotopes.

For the isotope  $^{151}\text{Eu}$  the experimental data have a scatter of approximately 20-30% and it is difficult to give preference to any particular author. An optimum description of the data of Refs [17] and [15] gives the following parameter evaluations performed by means of the maximum probability methods  $S_1 = 0.114 \pm 0.033$ ;  $S_2 = 3.5 \pm 1.0$ ;  $S_\gamma = 4926 \pm 500$ ; it also yields a high value of  $\sigma_c$  (1 MeV), equal to 1.6 b. Matching these values to the data obtained by Kononov [16], Czirr [13] and Hockenbury [14] yields parameters close to those obtained in Ref. [16]. The optimum aggregate description of the data of five authors, i.e. the description giving the closest agreement, yields parameters which are adopted as recommended and it is by means of these

parameters that the calculated curve in Fig. 4 is obtained. The isotope  $^{151}\text{Eu}$  is not a particularly important fission product and does not, therefore, receive adequate attention in Refs [1-5]. Consequently, a detailed comparison of the different evaluations is not possible.

The experimental situation with respect to  $^{153}\text{Eu}$  is similar to that of the preceding nucleus, although the two sets of data [13,16] and [14,15,17] differ not only in terms of energy dependence but also in absolute values. It is to be expected that the process of matching the theoretical curves to the data of different authors will yield different parameters. In particular, description of the data of Refs [13] and [16] yields parameters which agree - within the limits of error - with the results of Ref. [16], while adjustment to the data of Refs [14,15,17] results in the values  $S_1 = 0.275 \pm 0.063$ ;  $S_2 = 3.45 \pm 0.52$ ; and  $S_\gamma = 1653 \pm 82$ . An attempt to describe the two groups of experimental data at a time gives similar values for the neutron strength functions, but a somewhat higher value for  $S_\gamma$  (see Table 2), the calculation being 20-30% higher than the other evaluations (see Fig. 5). It should be noted that virtually all the absolute-value evaluations are normalized to the data of Ref. [11] at an energy of approximately 10 keV and consequently, while describing the results of Ref. [11] and others [12-15,17] up to energies of 30-50 keV, consistently fall below the experimental data beyond such energies.

The calculated curve for  $^{155}\text{Eu}$  is obtained in the same way as that for  $^{151}\text{Sm}$ . At low energies all the evaluations agree within limits of 30%, but at  $E_n = 1000$  keV they vary considerably (see Fig. 6 and Table 2). Below the error correlation matrices are set out for the optimum parameters (W), while Tables 3 and 4 set out the sensitivity coefficients of the capture cross-sections to the strength functions and the accuracy of the evaluated cross-sections.

### Conclusion

An evaluation has been made of the fast-neutron radiative capture cross-section for six fission products - the odd samarium and europium isotopes  $^{147},^{149},^{151}\text{Sm}$  and  $^{151},^{153},^{155}\text{Eu}$ . The mean recommended resonance parameters (neutron and radiative strength functions) are given, together with the covariational matrix of the parameter errors. The error in the evaluated cross-section curves was found to be approximately 5-15%.



Analysis of the available experimental data, theoretical calculations and other evaluations led to the following conclusions:

- There continues to be insufficient experimental information on fission products. There is need to perform new measurements of  $\sigma_c(E_n)$  over a wide range of neutron energies, primarily for  $^{147}\text{Sm}$  and  $^{153}\text{Eu}$ . The possibility must be explored of experimentally determining the value of  $\sigma_c$  for radioactive fission product isotopes such as  $^{151}\text{Sm}$  and  $^{155}\text{Eu}$ ;
- The available experimental data and various evaluations for the cross-sections of fast-neutron capture by fission products fall short at present of the level of accuracy required. Furthermore, for almost all the samarium and europium isotopes under investigation they disagree, the spread being 20-30%. This discrepancy increases appreciably in the high neutron energy region (around 1 MeV);
- The discrepancy in the evaluations within the energy range 1-100 keV is clearly due to their normalization to different sets of experimental data, which are not always in agreement;
- The mismatch between the various evaluations at high neutron energies is probably due to the different values adopted for the p- and d-wave neutron strength functions, the different level schemes used and the divergent notions on which the models are based. In Refs [2-5]  $S_2$  is calculated according to the optical model of the nucleus, the preferred type usually being the spherical model. The values of  $S_1$  are also calculated according to the optical model because the rare-earth nuclei are generally considerably deformed. However, in order to calculate the strength functions in the case of the latter, it is necessary to apply the non-spherical optical model or the coupled-channel method. It has been found that the values of  $S_1$  and  $S_2$ , calculated according to the spherical optical model and the coupled-channel method in the region  $A = 140-180$  [minimum  $S_1(A)$  and maximum 3D-shape resonance in  $S_2(A)$ ], differ markedly. The completed evaluation does not have this drawback: it is entirely based on the experimental systematics for  $S_1(A)$ ;

- When evaluating  $\sigma_c$  for fission products one needs to perform integral measurements in order to increase the reliability and accuracy of the recommended data. This approach in ENDF/B-V for  $^{147,149}\text{Sm}$  resulted at  $E_n = 1-1000$  keV in a consistent increase by a factor of 1.5 in the radiative capture cross-sections, an increase confirmed by the present evaluation;
- For a fuller understanding of the results of each evaluation together with the corresponding calculated cross-section curve and recommended parameter values there is need to formulate a covariational matrix of the errors of these parameters and the error of the evaluated curve.

REFERENCES

- [1] England T.R., Schenter R.E. ENDF/B-IV fission product files. LA-6116-MS/ENDF-223/, 1975. Schenter R.E., England T.R. ENDF/B-5 fission product cross-section evaluation: Proc. of the specialists' meeting on neutron cross-sections of fission product nuclei. Dec. 12-14, 1979. Bologna, Italy, p.253.
- [2] Kikuchi Y., Nakagawa T., Matsumoto H. e.a. Neutron cross-sections of 28 fission product nuclides adopted in JENDL-1. JAERI 1268, 1981.
- [3] Gruppelaar H. Tables of ECN-2 fission product cross-section evaluation. V.1-3. ECN-13, 1975; ECN-33, 1977; ECN-65, 1979; Gruppelaar H., Dekker J.W.M. ECN-24, 1977.
- [4] Ribon P., Fort E., Krebs J. Quoc Thuong T. CEA-N-1832, 1975.
- [5] Montagnati A., Panini G.C., Vaccari M. RT/FI(78)16, RT/FI(78)23, CNEN-RT/FI(80)1.
- [6] USACHEV, L.N., BOBKOV, Yu.G., Teoriya vozmushchenij i planirovanie ehksperimenta v probleme yadernykh dannykh dlya reaktorov (Perturbation theory and experiment planning as applied to nuclear data for reactors), Atomizdat, Moscow (1980): BOBKOV, Yu.G., KRIVTSOV, A.S., USACHEV, L.N., Voprosy atomnoj nauki i tekhniki (Questions of atomic science and technology), Ser. Yadernye Konstanty (Nuclear Constants Series) 3 (38) (1980) 3.
- [7] TROYANOV, M.F., At. Ehnerg. 50 2 (1981) 102.
- [8] ALEKSEEV, P.N., MANTUROV, G.N., NIKOLAEV, M.N., ibid. 49 4 (1980) 221.
- [9] Johnson A.E., Silbert M.G., Marshall H.H. Phys. Rev., 1959, v. 116, p.927.
- [10] Macklin R.L., Gibbons J.H., Inada T. Nature, 1963, v.197, p. 369.
- [11] KONKS, V.A., POPOV, Yu.P., FENIN, Yu.I., Yad. Fiz. 7 3 (1968) 310.
- [12] Harlow M.V., Schelberg A.D., Tatro L.D. e.a. 2nd Conference on nuclear cross-sections and technology. Washington D.C., 1968, p.837.
- [13] Csirr J.B. ENL-325, 3d ed., 1976, v.2, p.338.
- [14] Hockenbury R.W., Knox H.R., Kaushal N.N. 4th conference on nuclear cross-sections and technology. Washington D.C., 1975, p. 905; Hockenbury R.W., Koste W.R., Shaw R.A. Bull. Amer. Phys. Soc., 1975, v.20, p.560.
- [15] Moran M.C., Endacott D.A., Jolly J.E. Ann. Nucl. Energy, 1976, v.3, p.399.
- [16] KONONOV, V.N., YURLOV, B.D., MANTUROV, G.N. et al., Voprosy atomnoj nauki i tekhniki, Ser. Yadernye Konstanty 22 (1976) 29.  
KONONOV, V.N., YURLOV, B.D., POLETAEV, E.D. et al., Yad. Fiz. 26 (1977) 947.
- [17] Mizumoto M., Asami A., Nakajima Y. e.a. J. Nucl. Sci. and Technol., 1979, v.16, p.711; Yamamoto N., Asami A. Proc. of the specialists' meeting on neutron cross-sections of fission product nuclei, Dec. 12-14, 1979, p.41.
- [18] Mizumoto M. Nucl. Phys., 1981, v.A357, p.90.
- [19] Chou-Jen-Chang, Werle H.J. J. Nucl. Energy, 1973, v. 27, p.811.
- [20] Lepine J.R.D., Douglas R.A., Maia H.A. Nucl. Phys., 1972, v.A196, p.83.
- [21] Macklin R.L., Gibbons J.H., Inada T. Phys. Rev., 1963, v.129, p.2695; Ibid., 1967, v.159, p.1007.
- [22] Fort E. Second advisory group meeting on fission product nuclear data. Petten, 1977, rep.7.
- [23] Gibbons J.H., Macklin R.L., Miller R.D. e.a. Phys. Rev., 1961, v.122, p.182.
- [24] Block R.C., Slaughter G.G., Weston L.W. Neutron time of flight meth. Brussel, 1961, p.203.
- [25] Poenitz W.P. Proceedings of the specialists' meeting on neutron cross-sections of fission product nuclei, Dec. 12-14, 1979, p.85.

- [26] Widder F. KIR-Bericht Nr. 217.
- [27] Mughabghab S.F., Garber D.I. Neutron cross-sections. V. 1. Resonance Parameters. BNL-325, 3d ed., 1973.
- [28] Fujino M., Takahashi P., Yamamoto H. J. Nucl. Sci. and Technol., 1976, v.13, p.566.
- [29] Garber D.I., Kinsey R.R. Neutron cross-sections. V. II. Curves, BNL-325, 3d ed., 1976.
- [30] Hauser W., Feshbach H. Phys. Rev., 1952, v.87, p.366; Moldauer P. Rev. Mod. Phys., 1971, v.36, p.1074.
- [31] KOSHCHEEV, V.N., SINITSA, V.V., Nejtronnaya Fizika (Neutron Physics) (Proc. 4th All-Union Conf. Neutron Physics, Kiev, 1977), Part 2, TsNIIatominform, Moscow, p. 70.
- [32] BLOKHIN, A.I., IGNATYUK, A.V., PLATONOV, V.P., TOLSTIKOV, V.A., Voprosy atomnoj nauki i tekhniki, Ser. Yadernye Konstanty 21 (1976) 3.
- [33] MANTUROV, G.N., NIKOLAEV, M.N., Pre-print FEhI-666, Obninsk (1976).
- [34] Seth K.K. Nucl. Data, 1966, v.A2, p.321.
- [35] Musgrove A.R. A compilation of s- and p-wave neutron strength function data. AABC/E277, 1973.
- [36] KONONOV, V.N., YURLOV, B.D. et al., p- i d-volnovye nejtronnnye silovye funktsii dlya yader redkozemel'noj oblasti (p- and d-wave neutron strength functions for nuclei in the rare-earth region), Nejtronnaya Fizika (Neutron Physics) (Proc. 4th All-Union Conf. Neutron Physics, Kiev, 1977), Part 2, TsNIIatominform, Moscow, p. 201.
- [37] YURLOV, B.D., Abstract of dissertation for the degree of Candidate (Master) of Physical and Mathematical Sciences, OIYaI, Dubna (1978).
- [38] KIROUAC, G.J., EILAND, H.M., Phys. Rev., 1975, v. C11, p. 895.
- [39] ANUFRIEV, V.A. et al., At. Ehnerg. 46 (1979) 158.
- [40] DOVBENKO, A.G., KONONOV, V.N., LUNEV, V.P., YURLOV, B.D., Pre-print FEhI-1045, Obninsk (1980).

Table 1

Summary of the experimental studies conducted to measure neutron capture cross-sections for samarium and europium odd isotopes

Reference	Energy, keV	Number of points	Neutron source	Method	Standard and flux monitor	Nuclei investigated
Johnsrud [9]	175-2500	14	EA	A	$\sigma_c^T(\text{Eu}) = 1400 \text{ b}$ $\sigma_f(^{235}\text{U})$	$^{151}\text{Eu}$
Macklin [10]	$30 \pm 7$	1	"	TFM, MR	$\sigma_c(\text{Ag}) = 951 \text{ mb}$ at $E_n = 30 \text{ keV}$ $^{10}\text{B}(n,\alpha\gamma)^7\text{Li}$	$^{147,149}\text{Sm}$
Konks [11]	0.001-40	86	SDT	SDT PC	Normalization to low-lying resonance	$^{63}\text{Eu}$ , $^{153}\text{Eu}$ , $^{151}\text{Eu}$ (calculated)
Harlow [12]	0.025-10	-	Nuclear	TFM, MR	Normalization to data of Ref. [12], $^6\text{Li}(n,\alpha)\text{T}$	$^{151,153}\text{Eu}$
Czirt [13]	0.2-12.5	98	LEA	TFM, ML	Normalization to resonance 7.44 eV $^{151}\text{Eu}$ $^{10}\text{B}(n,\alpha\gamma)^7\text{Li}$	$^{63}\text{Eu}$ , $^{151}\text{Eu}$ , $^{153}\text{Eu}$ (calculated)
Hockenbury [14]	6.3-300; 0.02-150	566	"	TFM LLSC	Normalization to resonance 31.3 eV $^{153}\text{Eu}$ $^{10}\text{B}(n,\alpha\gamma)^7\text{Li}$	$^{151,153}\text{Eu}$ , $^{149}\text{Sm}$
Moxon [15]	0.1-100	27	"	TFM, MR	Normalization to low-lying resonance $^{10}\text{B}(n,\alpha\gamma)^7\text{Li}$	$^{151,153}\text{Eu}$ , $^{63}\text{Eu}$ (calculated)
Kononov [16]	5-350	75	EA	TFM LSC	$\sigma_c(\text{Au}) = 596 \text{ mb}$ at $E_n = 30 \text{ keV}$ $^{10}\text{B}(n,\alpha\gamma)^7\text{Li}$	$^{147,149}\text{Sm}$ , $^{62}\text{Sm}$ , $^{151,153}\text{Eu}$ , $^{63}\text{Eu}$

Table 1 (continued)

Reference	Energy keV	Number of points	Neutron source	Method	Standard and flux monitor	Nuclei investigated
Mizumoto [17]	3-300	23	LEA	TFM LLSC	Normalization to saturated resonances	$^{151,153}\text{Eu}$ , $^{63}\text{Eu}$
Mizumoto [18]	1.5-300	30	"	LLSC	As above $^6\text{Li}(N,\alpha)\text{T}$ $^{10}\text{B}(n,\alpha\gamma)^7\text{Li}$	$^{147,149}\text{Sm}$

Legend: TFM - time-of-flight method; EA - electrostatic accelerator; LEA - linear electron accelerator; SDT - lead slowing-down time spectrometer; MR - Moxon-Rae detector; ML - Mayer-Leibnitz detector; LLSC - large liquid scintillation counter; PC - proportional counter; SC - scintillation counter; LSC - liquid scintillation counter; A - activation method.

Table 2  
Calculated parameters

Parameter	[27]	[1]	[4]	[5]	[3]	[2]	Present study
For $^{147}\text{Sm}$							
$10^4 s_0$	$4,6 \pm 0,4$	-	-	4,3	4,3	4,02	$4,6 \pm 0,4$
$10^4 s_1$	-	-	-	1,0	1,8	0,52	$0,150 \pm 0,045$
$10^4 s_2$	-	-	-	-	-	-	$1,30 \pm 0,26$
$\bar{\Gamma}_T$ , MeV	$67 \pm 2$	63	-	84	100	67	- -
$\bar{D}_{\text{obs}}$ , eV	$7,4 \pm 0,7$	6,7	-	5,3	6,3	4,26	- -
$10^4 s_T$	91	94	-	158	159	157	$420 \pm 84$
$R^0, \theta$	-	6,366	-	5,8	6,366	4,45	7,5
$a$ , $\text{MeV}^{-1}$	-	-	-	19,5	21,0	21,41	18,79
$\sigma_c$ (at 30 keV), mb	-	776	-	848	1221	1005	1,650
$\sigma_t$ (at 30 keV), mb	-	19100	-	14100	15000	12100	14280
For $^{149}\text{Sm}$							
$10^4 s_0$	$5,1 \pm 0,9$	-	5,2	5,5	5,1	3,88	$5,1 \pm 0,9$
$10^4 s_1$	-	-	0,6	0,4	1,8	0,54	$0,300 \pm 0,045$
$10^4 s_2$	-	-	-	-	-	-	$1,500 \pm 0,225$
$\bar{\Gamma}_T$ , MeV	$60,5 \pm 5$	62	60,5	64	76	61	- -
$\bar{D}_{\text{obs}}$ , eV	$2,3 \pm 0,3$	2,3	1,95	2,3	2,0	1,63	- -
$10^4 s_T$	263	277	310	278	380	374	$900 \pm 27$

Table 2 (continued)

Parameter	[27]	[1]	[4]	[5]	[3]	[2]	Present study
$R^1, \theta$	-	5,093	6,6	5,093	5,09	8,4	7,5
$a, \text{MeV}^{-1}$	-	-	-	22,75	23,5	20,8	20,10
$\sigma_c(\text{at } 30 \text{ keV}), \text{mb}$	-	1620	1496	1310	1947	1645	2602
$\sigma_t(\text{at } 30 \text{ keV}), \text{mb}$	-	13300	-	12000	16600	11800	14960
For $^{151}\text{Sm}$							
$10^4 s_0$	$4,0 \pm 1,8$	-	3,5	3,68	3,65	3,8	$3,65 \pm 0,48$
$10^4 s_1$	-	-	0,8	0,5	1,2	0,55	$0,250 \pm 0,075$
$10^4 s_2$	-	-	-	-	-	-	$4,0 \pm 0,8$
$\bar{F}_p, \text{MeV}$	$75 \pm 4$	75	78	96	96	75	-
$\bar{D}_{\text{obs}}, \text{eV}$	$1,3 \pm 0,2$	1,3	0,9	1,7	1,72	1,5	-
$10^4 s_p$	577	570	667	565	558	500	$1200 \pm 120$
$R^1, \theta$	-	6,42	6,65	7,46	6,42	8,35	8,0
$a, \text{MeV}^{-1}$	-	-	-	25,9	28,88	21,26	20,20
$\sigma_c(\text{at } 30 \text{ keV}), \text{mb}$	-	1967	2457	2011	2062	1825	2594
$\sigma_t(\text{at } 30 \text{ keV}), \text{mb}$	-	13900	-	11800	14600	11700	12811
For $^{151}\text{Eu}$							
$10^4 s_0$	$3,7 \pm 0,5$	-	-	-	-	-	$3,7 \pm 0,5$
$10^4 s_1$	$1,0 \pm 0,8$	-	-	-	-	-	$0,10 \pm 0,03$
$10^4 s_2$	-	-	-	-	-	-	$2,5 \pm 0,5$
$\bar{F}_p, \text{MeV}$	-	92	-	90	-	88	-
$\bar{D}_{\text{obs}}, \text{eV}$	$0,7 \pm 0,2$	0,655	-	0,974	-	0,72	-
$10^4 s_p$	-	1400	-	-	-	-	$3200 \pm 320$
$R^1, \theta$	$8,8 \pm 0,4$	-	-	-	-	-	7,68
$a, \text{MeV}^{-1}$	-	23,28	-	-	-	-	20,26
$\sigma_c(\text{at } 30 \text{ keV}), \text{mb}$	-	3500	-	-	-	-	4092
$\sigma_t(\text{at } 30 \text{ keV}), \text{mb}$	-	-	-	-	-	-	13371
For $^{153}\text{Eu}$							
$10^4 s_0$	$2,5 \pm 0,9$	3,54	-	2,8	-	4,2	$2,5 \pm 0,2$
$10^4 s_1$	$0,6 \pm 0,4$	1,43	-	1,0	-	0,49	$0,24 \pm 0,07$
$10^4 s_2$	-	-	-	-	-	-	$0,40 \pm 0,88$
$\bar{F}_p, \text{MeV}$	$94 \pm 1$	94,8	-	90	-	94	-
$\bar{D}_{\text{obs}}, \text{eV}$	$1,3 \pm 0,2$	1,3	-	1,05	-	1,46	-
$10^4 s_p$	723	729	-	857	-	644	$2100 \pm 210$
$R^1, \theta$	$8,8 \pm 0,4$	8,8	-	8,8	-	8,8	8,16
$a, \text{MeV}^{-1}$	-	-	-	25,7	-	21,81	20,44
$\sigma_c(\text{at } 30 \text{ keV}), \text{mb}$	-	2430	-	2674	-	2566	3105



Table 2 (concluded)

Parameter	[27]	[17]	[4]	[5]	[3]	[2]	Present study
$\sigma_t$ (at 30 keV), mb	-	14100	-	13900	-	12600	12539
			For $^{155}\text{Eu}$				
$10^4 s_0$	-	-	-	2,2	-	4,13	$2,35 \pm 0,47$
$10^4 s_1$	-	-	-	0,1	-	0,49	$0,65 \pm 0,19$
$10^4 s_2$	-	-	-	-	-	-	$35 \pm 0,7$
$\bar{r}_p$ , MeV	-	-	-	129	-	100	-
$\bar{D}_{\text{obs}}$ , eV	-	-	-	0,92	-	2,5	-
$10^4 s_p$	-	407	-	1400	-	400	$2200 \pm 220$
$R^*$ , Å	-	6,48	-	8,0	-	8,15	8,2
$a$ , MeV $^{-1}$	-	-	-	24,8	-	20,85	18,0
$\sigma_c$ (at 30 keV), mb	-	2163	-	2556	-	1885	3148
$\sigma_t$ (at 30 keV), mb	-	12500	-	12200	-	12500	12503

Table 3

Sensitivity coefficients of the capture cross-sections to force functions

$$\left( H_{S_c} = \frac{S_c}{\sigma_c} \frac{\partial \sigma_c}{\partial S_c}, H_{S_f} = \frac{S_f}{\sigma_c} \frac{\partial \sigma_c}{\partial S_f} \right) \text{ at individual energy points}$$

Coefficient of sensitivity	<sup>147</sup> Sm			<sup>149</sup> Sm			<sup>151</sup> Sm		
	Energy, keV			Energy, keV			Energy, keV		
	I	100	1000	I	100	1000	I	100	1000
H <sub>S<sub>c</sub>0</sub>	0,58	0,10	-0,15	0,71	0,10	-0,37	0,82	-0,00	-0,20
H <sub>S<sub>c</sub>1</sub>	0,00	0,13	0,15	0,00	0,16	0,20	0,00	0,16	0,16
H <sub>S<sub>c</sub>2</sub>	0,00	0,07	0,25	0,00	0,06	0,28	0,00	0,10	0,15
H <sub>S<sub>f</sub></sub>	0,39	0,63	0,54	0,25	0,55	0,63	0,15	0,59	0,76
Coefficient of sensitivity	<sup>151</sup> Su			<sup>153</sup> Su			<sup>155</sup> Su		
	Energy, keV			Energy, keV			Energy, keV		
	I	100	1000	I	100	1000	I	100	1000
H <sub>S<sub>c</sub>0</sub>	0,90	0,34	-0,04	0,91	0,35	-0,07	0,92	0,34	-0,05
H <sub>S<sub>c</sub>1</sub>	0,00	0,04	0,05	0,00	0,11	0,07	0,00	0,21	0,13
H <sub>S<sub>c</sub>2</sub>	0,00	0,05	0,35	0,00	0,11	0,13	0,00	0,06	0,27
H <sub>S<sub>f</sub></sub>	0,07	0,36	0,32	0,07	0,31	0,56	0,06	0,28	0,53

Table 4

Accuracy of the evaluated fast-neutron radiative  
capture cross-sections, %

Energy, keV	$^{147}\text{Sm}$	$^{149}\text{Sm}$	$^{151}\text{Sm}$	$^{151}\text{Eu}$	$^{153}\text{Eu}$	$^{155}\text{Eu}$
1	17.1	12.9	11.1	11.7	7.3	19.3
100	18.0	2.6	2.1	5.6	4.0	10.9
1000	17.7	8.0	15.0	7.1	5.1	17.6

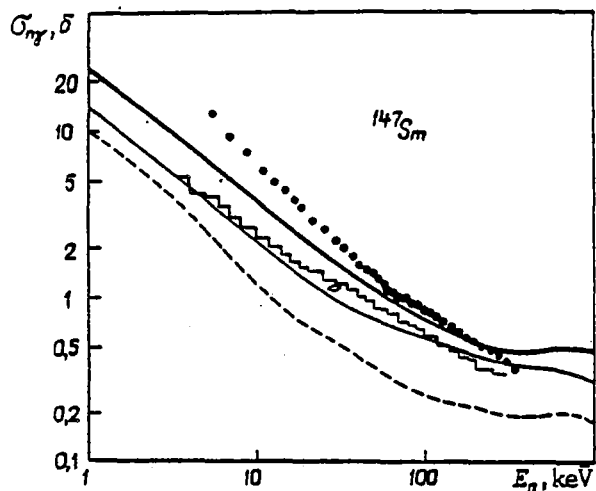


Fig. 1. Neutron radiative capture cross-section for  $^{147}\text{Sm}$ . Experimental data from the following studies:  $\bullet$  - [16];  $\square$  - [18];  $\circ$  - [10]. Calculations:  $\text{—}$  - present evaluation;  $\text{---}$  - JENDL-1 [2];  $\text{- - -}$  at  $S_\gamma = S_{\gamma\text{res}}$ .

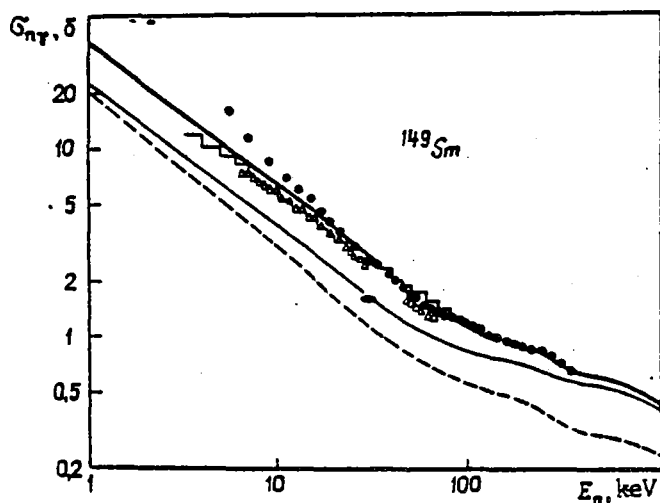


Fig. 2. Neutron radiative capture cross-sections for  $^{149}\text{Sm}$ . Experimental data from the following studies:  $\bullet$  - [16];  $\square$  - [18];  $\circ$  - [10];  $\Delta$  - [14]. Calculations:  $\text{—}$  - present evaluation;  $\text{---}$  - JENDL-1 [2];  $\text{- - -}$  at  $S_\gamma = S_{\gamma\text{res}}$ .

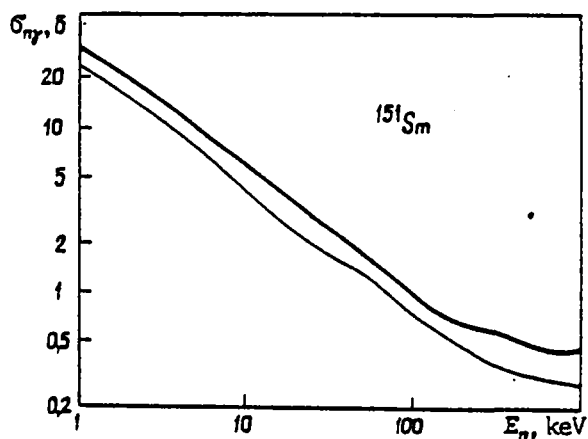


Fig. 3. Neutron radiative capture cross-section for  $^{151}\text{Sm}$ . Calculations: — - present evaluation; - - - JENDL-1 [2].

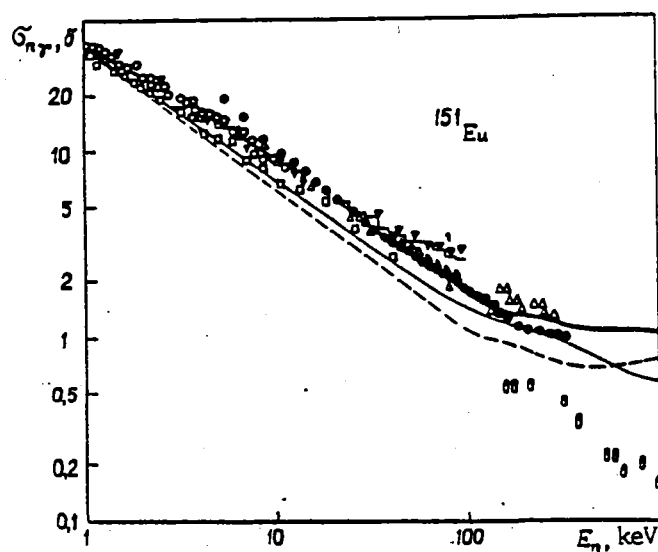


Fig. 4. Neutron radiative capture cross-section for  $^{151}\text{Eu}$ . Experimental data from the following studies:  $\bullet$  - [16];  $\square$  - [17];  $\circ$  - [13];  $\Delta$  - [14];  $\blacktriangledown$  - [15];  $\square$  - [11];  $\circ$  - [9]. Calculations: — - present evaluation; - - - calculation at  $S_\gamma = S_{\gamma,\text{res}}$ ; — - JENDL-1 [2].

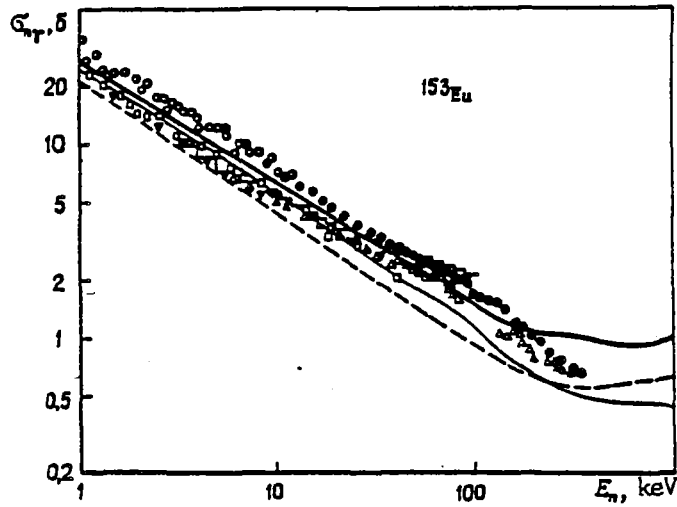


Fig. 5. Neutron radiative capture cross-section for  $^{153}\text{Eu}$ . Experimental data from the following studies:  $\bullet$  - [16];  $\square$  - [17];  $\circ$  - [13];  $\Delta$  - [14];  $\blacktriangledown$  - [15];  $\square$  - [11]. Calculations:  $\text{---}$  - present evaluation;  $\text{—}$  - JENDL-1 [2];  $\text{- - -}$  at  $S_\gamma = S_{\gamma\text{res}}$ .

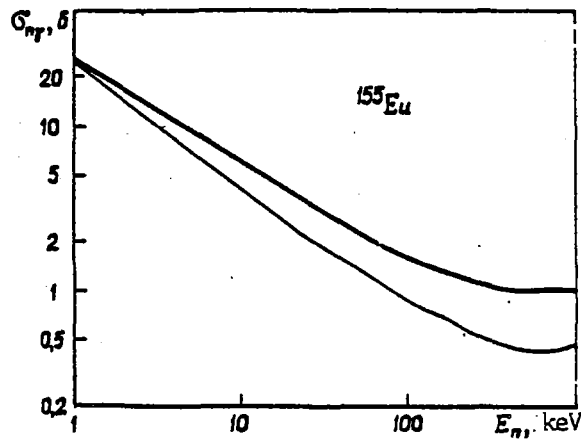


Fig. 6. Neutron radiative capture cross-section for  $^{155}\text{Eu}$ . Calculations:  $\text{---}$  - present evaluation;  $\text{—}$  - JENDL-1 [2].

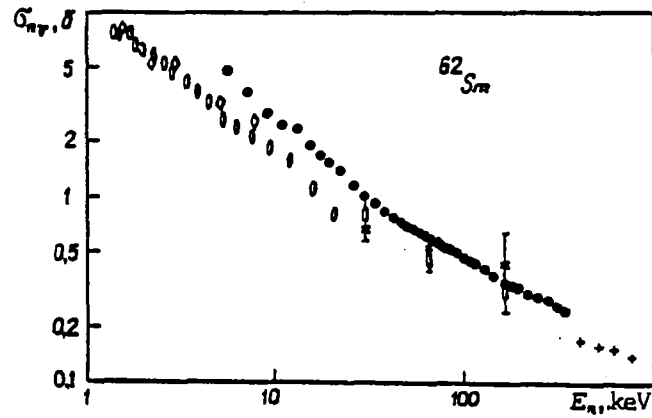


Fig. 7. Neutron radiative capture cross-section for natural samarium. Experimental data from the following studies: ● - [16]; ○ - [19]; x - [20]; □ - [23]; ◇ - [24]; + - [25].

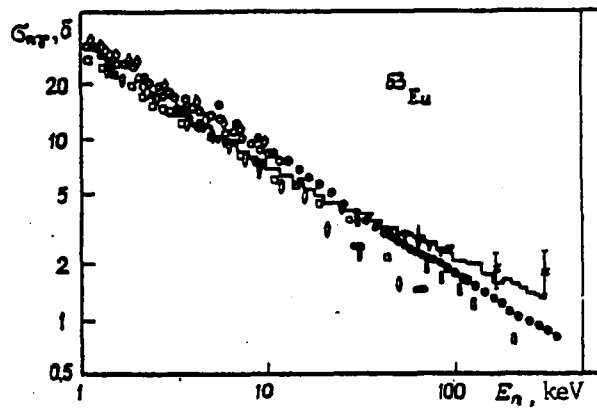


Fig. 8. Neutron radiative capture cross-section for natural europium. Experimental data from the following studies: ● - [16]; ○ - [13]; ◧ - [17]; □ - [11]; ▼ - [15]; ○ - [19]; ◇ - [24]; x - [20]; □○ - [21].

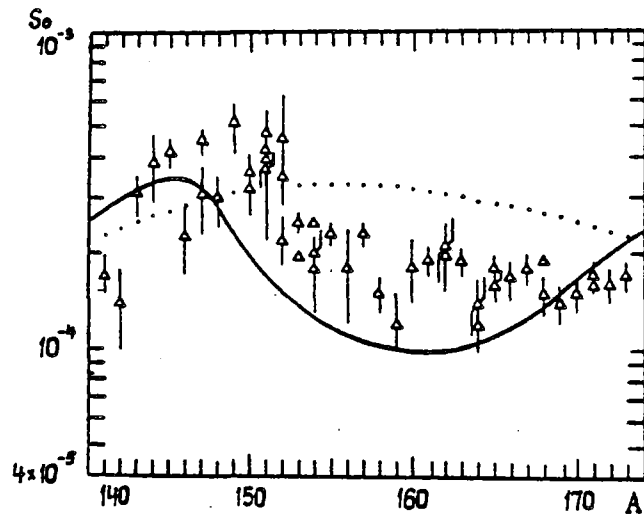


Fig. 9. Fragment of the dependence  $S_0(A)$  in the region  $A = 140-170$ .  
Experimental data:  $\triangle$  - from Ref. [27]. Calculations:  
— - coupled-channel method; .... - spherical optical model  
[37,40].



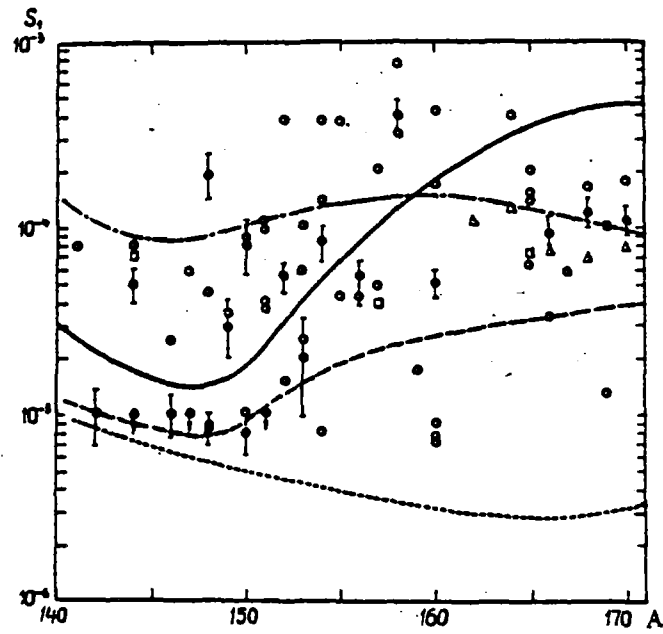


Fig. 10. Fragment of the dependence  $S_1$  (A) in the region  $A = 140-170$ .  
Experimental data:  $\phi$  - Refs [36,37];  $\circ$  - analysis of capture cross-sections;  $\square$  - analysis of mean full cross-sections;  $\Delta$  - analysis of the isolated resonance region. Calculations:  $-\cdot-\cdot-$  - non-spherical optical model of Baka and Peri (?) [27];  $-\cdot-\cdot-$ ,  $---$  - coupled-channel method;  $\dots$  - spherical optical method [37,40].

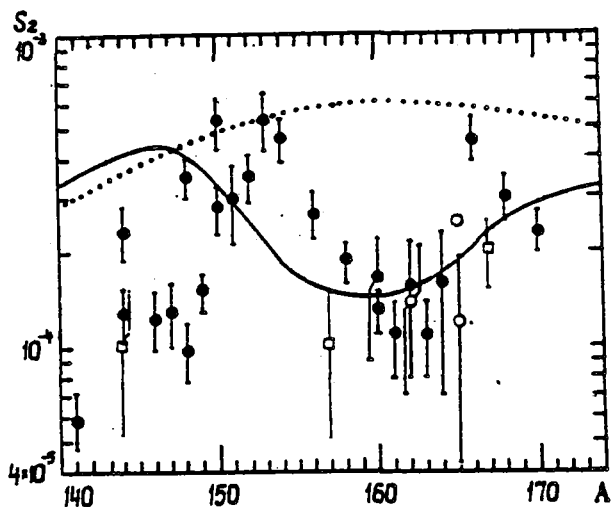


Fig. 11. Fragment of the dependence  $S_2$  (A) in the region  $A = 140-170$ .  
Experimental data:  $\bullet$  - Refs [36,37];  $\circ$  - analysis of capture cross-sections;  $\square$  - analysis of mean full cross-sections.  
Calculations: — - coupled-channel method; .... - spherical optical method [37,40].

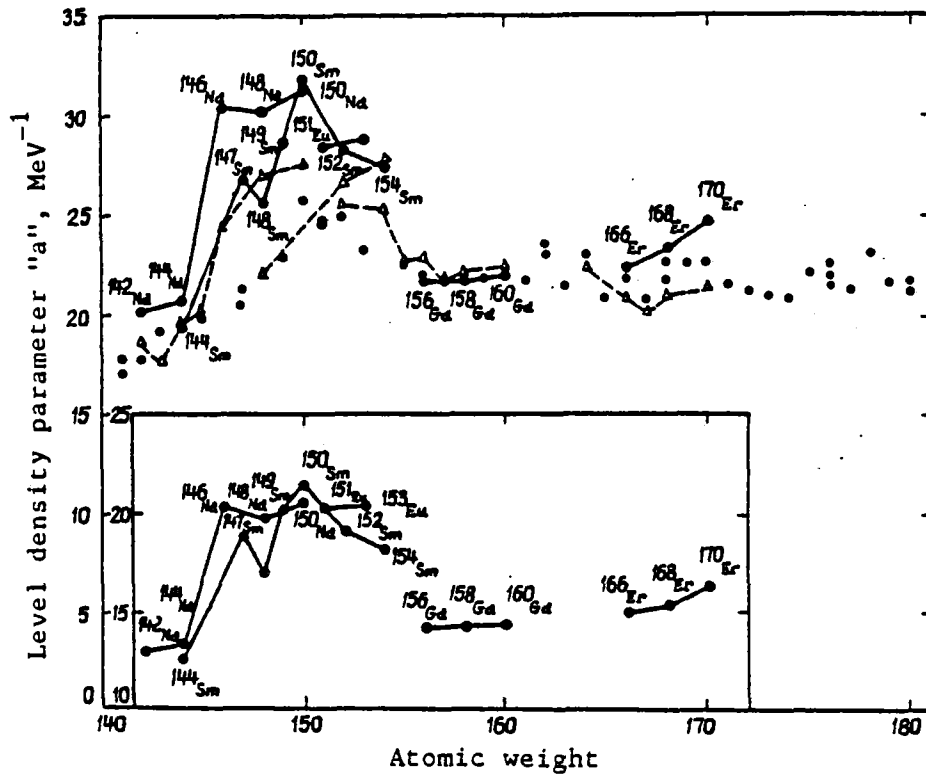


Fig. 12. Fragment of the dependence of the level density parameter "a" in the region  $A = 140-180$  [37]. Inset: data taking account of the collective motion of the nuclei.

UDK 539.173

COVARIANCE MATRIX OF EXPERIMENTAL DATA ON THE ENERGY DEPENDENCE  
OF  $\bar{\nu}_p$  FOR NEUTRON-INDUCED FISSION OF THE NUCLEI  
 $^{232}\text{Th}$ ,  $^{236}\text{U}$ ,  $^{238}\text{U}$ ,  $^{237}\text{Np}$

V.V. Malinovskij, B.D. Kuz'minov, V.G. Vorob'eva

The problems of evaluating nuclear data involve the need to take accurate account of all the errors in the experimental results used and the correlations thereof. This means that the experimentalist must introduce a covariance matrix of the data.

The purpose of the present study is to evaluate the error matrix in the measurement of the energy dependence of the average number of prompt neutrons  $\bar{\nu}_p$  in the fission of nuclei induced by fast neutrons. We consider the method of measuring  $\bar{\nu}_p$  in relation to the standard - the average number of prompt neutrons in the spontaneous fission of  $^{252}\text{Cf}$ . The neutron detector was a set of  $^3\text{He}$  counters in a polyethylene moderator. The measurements were made on a monoenergetic neutron beam obtained from the reactions  $T(p,n)$  and  $D(d,n)$  in an electrostatic accelerator operating under steady-state conditions [1]. However, the calculation performed may possibly be of interest for other methods as well. The method of measuring  $\bar{\nu}_p$  considered here is described in detail in the study of Vorob'eva and associates [1] and therefore we shall deal below only with the details relating to the calculations of the error matrix.

The value of  $\bar{\nu}_p$  determined in the measurements is equal to

$$\nu = \nu_0 k_c k_a f(\nu, \nu_0) \beta, \quad (1)$$

(for the sake of simplicity in notation we shall omit the subscript p and the average sign in the operations), where  $\nu$  is the average number of prompt neutrons in fast-neutron-induced fission;  $\nu_0$  is the average number of prompt neutrons in spontaneous fission of the standard -  $^{252}\text{Cf}$ ;  $\beta$  is the ratio obtained experimentally, after subtraction of the background, of the values of the average number of prompt fission neutrons for the nucleus under study and for californium;  $k_c$ ,  $k_a$  and  $f(\nu, \nu_0)$  are various correction factors.

The procedure for subtracting background in these measurements is a statistical one and depends on the specific conditions of each series of measurements in the accelerator. This is dealt with in detail in the paper of

Frehaut [2]. The magnitude  $\beta$  represents the ratio of the numbers - corrected for background - of the neutron detector reading. For this reason the error is statistical in nature. The statistical error of the measurements referred to in Refs [1,3,4] is determined by the error of  $\beta$ .

The term  $k_c$  represents corrections taken as constants throughout the entire energy range of measurements for the particular element. These include corrections allowing for: (1) the dependence of fission neutron recording efficiency on the position of the fissionable layers on the axis of the neutron detector; (2) the difference between the diameters of the layers of  $^{252}\text{Cf}$  and of the nucleus under study; (3) the dependence of the number of recorded neutrons on the efficiency of fission fragment recording; (4) the difference in probabilities of complete slowing-down in the layer of the fissionable substance for fragments of different kinetic energy.

The term  $k_a$  includes corrections whose magnitude is determined either individually in each series of measurements or for the given neutron energy. These are corrections for: counting errors relating to pulses from fission neutrons in the case of coincidence with background pulses, the counting of spontaneous fissions or of pulse pile-ups from alpha particles, background-neutron-induced fission when the  $\text{D}(d,n)$  reaction is used. The correction for the difference in the angular distributions of fragments in the fission of the nuclei of  $^{252}\text{Cf}$  and the element under study, by reason of its nature, also belongs here. However, in Refs [1,4] this correction was assumed to be equal to  $1.000 \pm 0.001$  in the entire range of energies. For this reason, a correspondingly small uncertainty is considered as a constant in the entire measurement range.

Lastly, the term  $f(\nu, \nu_0)$  takes into account the corrections for the difference in energy spectra of the fission neutrons of the isotope being studied and  $^{252}\text{Cf}$  and for the errors in counting pulses from fission neutrons due to coincidence with one another within the limits of detector dead time. As the two corrections are small, and their dependence on the difference of  $\nu_p$  for the isotope under study and  $^{252}\text{Cf}$  is close to linear, the total correction is satisfactorily described by the expression

$$f(\nu, \nu_0) = 1 + \beta \frac{\nu - \nu_0}{\nu_0}, \quad (2)$$

where the coefficient  $b$  is determined with satisfactory accuracy from a large number of points and is equal to 0.1094.

In equation (1) all the factors except  $\nu_0$  and  $f$  are independent. As the expression for  $\nu$  (1) is a product, it is convenient to calculate all the terms of the covariance matrix in relative units. It follows from this that the diagonal term is

$$\frac{\overline{(\delta\nu_i)^2}}{\nu_i^2} = \frac{\overline{(\delta\nu_0)^2}}{\nu_0^2} + \frac{\overline{(\delta k_c)^2}}{k_c^2} + \frac{\overline{(\delta k_a)^2}}{k_a^2} + \frac{\overline{(\delta f_i)^2}}{f_i^2} + \frac{\overline{(\delta\beta_i)^2}}{(\beta_i)^2} \quad (3)$$

and the non-diagonal term is

$$\frac{\overline{\delta\nu_i \delta\nu_j}}{\nu_i \nu_j} = \frac{\text{COV}(\nu_i, \nu_j)}{\nu_i \nu_j} = \frac{\overline{(\delta\nu_0)^2}}{\nu_0^2} + \frac{\overline{(\delta k_c)^2}}{k_c^2} + \frac{\overline{\delta f_i \delta f_j}}{f_i f_j} \quad (4)$$

It is obvious that the terms corresponding to the values  $k_a$  and  $\beta$  are lacking in the expression for the non-diagonal term of the matrix since they are determined independently for the different intervals of energy dependence. For estimating the variations of  $f$  we take advantage of the explicit expression (2) and, discarding terms with  $(\delta b)$ , since  $\delta b \ll \delta\nu$ , we get:

$$\frac{\overline{(\delta f_i)^2}}{f_i^2} = \frac{1}{f^2} \left( \overline{(\delta\nu)^2} \left(\frac{b}{\nu_0}\right)^2 + \frac{b^2 \nu^2}{\nu_0^4} \overline{(\delta\nu_0)^2} - 2\overline{\delta\nu \delta\nu_0} \frac{b^2 \nu}{\nu_0^3} \right) \quad (5)$$

and

$$\frac{\overline{\delta f_i \delta f_j}}{f_i f_j} = \frac{b^2}{f_i f_j} \frac{\nu_i \nu_j}{\nu_0^2} \left( \frac{\overline{\delta\nu_i \delta\nu_j}}{\nu_i \nu_j} + \frac{\overline{(\delta\nu_0)^2}}{\nu_0^2} - 2 \frac{\overline{\delta\nu_i \delta\nu_0}}{\nu_i \nu_0} \right) \quad (6)$$

It is obvious that  $\overline{(\delta\nu_i \delta\nu_0)} / (\nu_i \nu_0) = \overline{(\delta\nu_0)^2} / \nu_0^2$ .

In expression (5), if we discard the final term with the minus sign in order to obtain the maximum estimate of errors and if we substitute the values obtained for  $\overline{(\delta f_i)^2}/f_i^2$  and  $\overline{(\delta f_i \delta f_j)}/(\bar{f}_i \bar{f}_j)$  in expressions (3) and (4), we get explicit expressions for the terms of the covariance matrix:

$$\frac{\overline{(\delta v)^2}}{v^2} = \left(1 - \frac{\beta^2}{f^2} \frac{v^2}{v_0^2}\right)^{-1} \left[ \left(1 + \frac{\beta^2}{f^2} \frac{v^2}{v_0^2}\right) \frac{\overline{(\delta v_0)^2}}{v_0^2} + \frac{\overline{(\delta k_c)^2}}{k_c^2} + \frac{\overline{(\delta k_a)^2}}{k_a^2} + \frac{\overline{(\delta \beta)^2}}{\beta^2} \right], \quad (7)$$

$$\frac{\overline{\delta v_i \delta v_j}}{v_i v_j} = \left(1 - \frac{\beta^2}{f_i f_j} \frac{v_i v_j}{v_0^2}\right)^{-1} \left[ \left(1 - \frac{\beta^2}{f_i f_j} \frac{v_i v_j}{v_0^2}\right) \frac{\overline{(\delta v_0)^2}}{v_0^2} + \frac{\overline{(\delta k_c)^2}}{k_c^2} \right]. \quad (8)$$

In the measurement results presented below, the standard error is not taken into account ( $\delta v_0 = 0$ ), since up to now there is no commonly accepted estimate of this error. For this reason the errors cited below are characteristic of the error of relative measurements. However, the complete expressions (7) and (8) are of interest in that the correlation properties of the data for  $\bar{v}_p$  require that allowance be made not only for  $v_0$ , but also - as a rule - for a term of the type  $f(v, v_0)$  in equation (1). Ordinarily, a purely statistical measurement error is cited separately in experimental data, which corresponds to the representation of a covariance matrix D in the following form:

$$D = S' \times I + D_{\text{sys}}, \quad (9)$$

where  $S'$  is the transposed column of values of the square of the statistical errors;  $I$  is the unit matrix;  $D_{\text{sys}}$  is the matrix, the elements of which are calculated without allowance for statistical error. Assuming that this will provide a more graphic representation of the individual components of the measurement error, we shall present the covariance matrices calculated in this way for the  $\bar{v}_p$  measurements data in the fast-neutron-induced fission of the nuclei  $^{232}\text{Th}$ ,  $^{236}\text{U}$ ,  $^{238}\text{U}$  and  $^{237}\text{Np}$ . In the calculations use was made of earlier estimates of the errors of individual corrections [1,4]. In the calculation of the covariance matrix for the  $\bar{v}_p$  measurements in the fission of  $^{237}\text{Np}$ , account was taken of the fact that the results of three series of measurements with different fission chambers were used.

It follows from expression (8) that in the present calculations the variation in the values of the non-diagonal elements of the  $D_{\text{sys}}$  matrix is limited by the factor  $b^2 \approx 0.01$  and can be considered constant to within two decimal places. For this reason, Table 1 shows only the diagonal terms of the  $D_{\text{sys}}$  matrix and one value of the non-diagonal element. An exception is made in the case of the data for  $^{237}\text{Np}$ , where the results of three series of measurements with different fission chambers are used. For this case the  $D_{\text{sys}}$  matrix is presented in its entirety in Table 2. In Table 1.3 we present the values of  $\bar{\nu}_p$  published earlier for the indicated neutron energy values and in relative units of the square of the statistical errors ( $S = \sigma_{\text{statistical}}^2 \cdot \nu^{-2}$ ), the diagonal terms of the  $D_{\text{sys}}$  matrix and the value of the diagonal element.

In some of the accompanying data a correlation matrix is used. There is no difficulty in deriving it from the covariance matrix:

$$a_{ij}(\text{corr}) = a_{ij}(\text{cov}) \left[ a_{ii}(\text{cov}) a_{jj}(\text{cov}) \right]^{-\frac{1}{2}}, \quad (10)$$

where  $a_{ij}(\text{corr})$  are the elements of the correlation matrix and  $a_{ij}(\text{cov})$  are the elements of the covariance matrix.

By way of an example, we present the correlation matrix of the  $\bar{\nu}_p$  measurements for  $^{237}\text{Np}$  (Table 4). In the calculation, the statistical error, according to expression (9) is included in the covariance matrix. The data for the measurement of  $\bar{\nu}_p$  in  $^{237}\text{Np}$  fission are of particular interest in this case since they were obtained in three experiments in which different fission chambers were used. The corresponding values are indicated in Table 3 by asterisks.



REFERENCES

- [1] VOROB'EVA, V.G., KUZ'MINOV, B.D., MALINOVSKIJ, V.V. et al., Voprosy atomnoj nauki i tekhniki. Ser. Yadernye konstanty, No. 3 (38) (1980) 44.
- [2] FREHAUT, J., In the book "Nejtronnaya fizika" (Neutron Physics: Proceedings of the Second All-Union Conference on Neutron Physics, Kiev, 28 May-1 June 1973), Obninsk, Institute of Physics and Power Engineering (FEI), 1974, part 3, pp. 165-176.
- [3] VOROB'EVA, V.G., KUZ'MINOV, B.D., MALINOVSKIJ, V.V. et al., Voprosy atomnoj nauki i tekhniki. Ser. Yadernye konstanty, No. 1 (40) (1981) 62.
- [4] MALINOVSKIJ, V.V., VOROB'EVA, V.G., KUZ'MINOV, B.D., Atomaya Ehnergiya, Vol. 53, No. 2, (1982) 83.

Paper submitted to editors on  
29 December 1982

Table 1. Results of  $\bar{\nu}$  measurements for  $^{232}\text{Th}$ ,  $^{236}\text{U}$ ,  $^{238}\text{U}$  and statistical measurement errors, relative units

Ser. No.	Neutron energy, MeV	$\bar{\nu}_p$	Square of statistical error $s \cdot 10^{-4}$	Diagonal element of covariance matrix $D_{\text{sys}} \cdot 10^{-4}$	Ser. No.	Neutron energy, MeV	$\bar{\nu}_p$	Square of statistical error $s \cdot 10^{-4}$	Diagonal element of covariance matrix $D_{\text{sys}} \cdot 10^{-4}$
For $^{232}\text{Th}$									
1	1,35	2,194	1,01	0,17	4	1,70	2,145	0,87	0,17
2	1,50	2,208	0,74	0,17	5	1,80	2,155	1,24	0,17
3	1,60	2,142	1,06	0,17	6	1,90	2,169	0,85	0,17
For $^{236}\text{U}$									
7	2,00	2,215	0,46	0,17	23	2,60	2,684	1,09	0,20
8	2,10	2,202	0,74	0,17	24	2,70	2,667	0,74	0,20
9	2,15	2,224	0,98	0,17	25	2,80	2,669	1,44	0,20
10	2,20	2,213	1,18	0,17	26	2,90	2,678	1,12	0,20
11	2,30	2,223	1,27	0,17	27	3,00	2,690	0,23	0,20
12	2,40	2,185	0,84	0,17	28	3,10	2,704	0,72	0,20
13	2,50	2,226	1,94	0,17	29	3,20	2,727	0,34	0,20
14	2,60	2,232	1,36	0,17	30	3,30	2,732	0,59	0,20
15	2,70	2,234	1,15	0,17	31	3,40	2,780	0,63	0,20
16	2,80	2,200	1,51	0,17	32	3,50	2,772	0,29	0,20
17	2,90	2,232	1,46	0,17	33	3,60	2,775	0,63	0,20
18	3,00	2,233	1,25	0,17	34	3,70	2,819	0,45	0,20
19	3,10	2,274	0,85	0,17	35	5,05	3,007	0,28	0,29
20	3,20	2,276	0,70	0,17	36	5,60	3,167	0,67	0,29
21	3,30	2,270	1,75	0,17	37	5,90	3,154	1,77	0,28
22	3,40	2,328	0,89	0,17	For $^{238}\text{U}$				
23	3,50	2,316	1,36	0,17	1	1,30	2,431	3,42	0,28
24	3,60	2,310	1,27	0,17	2	1,40	2,458	2,92	0,28
25	3,70	2,387	3,40	0,17	3	1,50	2,473	0,72	0,25
26	5,60	2,683	1,25	0,18	4	1,60	2,533	0,56	0,25
27	5,90	2,689	0,67	0,26	5	1,70	2,510	1,44	0,25
28	6,35	2,887	0,81	0,26	6	1,75	2,810	0,29	0,25
For $^{236}\text{U}$									
7	0,80	2,451	1,40	0,20	7	1,80	2,537	0,56	0,25
8	0,85	2,446	1,20	0,20	8	1,90	2,547	0,56	0,25
9	0,90	2,434	0,82	0,20	9	2,00	2,565	0,34	0,25
10	0,95	2,430	0,90	0,20	10	2,10	2,613	1,00	0,28
11	1,00	2,465	1,79	0,20	11	2,20	2,625	0,52	0,25
12	1,10	2,472	0,79	0,20	12	2,30	2,655	0,31	0,25
13	1,20	2,501	0,46	0,20	13	2,40	2,587	0,34	0,25
14	1,30	2,469	1,48	0,20	14	2,50	2,632	0,32	0,25
15	1,35	2,476	1,57	0,20	15	2,60	2,638	0,52	0,25
16	1,40	2,480	0,37	0,20	16	2,70	2,661	0,74	0,25
17	1,50	2,514	0,63	0,20	17	2,80	2,687	0,17	0,25
18	1,60	2,515	0,46	0,20	18	2,90	2,693	0,32	0,25
19	1,70	2,518	0,83	0,20	19	3,00	2,683	0,31	0,25
20	1,80	2,556	1,04	0,20	20	3,10	2,693	0,72	0,25
21	1,90	2,549	0,22	0,20	21	3,20	2,735	0,30	0,25
22	2,00	2,545	1,89	0,20	22	3,30	2,765	0,29	0,25
23	2,10	2,575	1,64	0,20	23	3,40	2,745	0,48	0,25
24	2,20	2,558	0,88	0,20	24	3,50	2,735	0,30	0,25
25	2,25	2,611	0,38	0,20	25	3,60	2,803	0,67	0,25
26	2,30	2,604	0,33	0,20	26	3,70	2,790	0,46	0,28
27	2,40	2,588	0,34	0,20	27	5,58	3,151	2,92	0,32
28	2,50	2,626	1,22	0,20	28	5,89	3,219	0,43	0,32

Note: The values of the non-diagonal elements of the D matrix are identical and equal: for  $^{232}\text{Th}$  -  $0.16 \cdot 10^{-4}$ ; for  $^{236}\text{U}$  -  $0.19 \cdot 10^{-4}$ ; for  $^{238}\text{U}$  -  $0.23 \cdot 10^{-4}$ .

Covariance matrix of data on  $\bar{v}_p$  in fission of  $^{237}\text{Np}$  (values,  $10^{-6}$ )

Table 2

Ser. No.	I	2	3	4	5	6	7	8	9	10	11	12	13	14	15	16	17	18	19	20	21	22	23	24	25	26	27	28	29	30	31
I	55																														
2	38	I53																													
3	38	38	55																												
4	38	38	38	55																											
5	38	38	38	38	55																										
6	38	38	38	38	38	45																									
7	I5	I5	I5	I5	I5	I5	4I																								
8	38	38	38	38	38	38	I5	62																							
9	38	38	38	38	38	38	I5	38	45																						
10	38	38	38	38	38	38	I5	38	38	44																					
11	38	38	38	38	38	38	I5	38	38	38	58																				
12	38	38	38	38	38	38	I5	38	38	38	38	46																			
13	I6	I6	I6	I6	I6	I6	I5	I6	I6	I6	I6	I6	26																		
14	38	38	38	38	38	38	I5	38	38	38	38	38	I6	48																	
15	38	38	38	38	38	38	I5	38	38	38	38	38	I6	38	48																
16	38	38	38	38	38	38	I5	38	38	38	38	38	I6	38	38	43															
17	38	38	38	38	38	38	I5	38	38	38	38	38	I6	38	38	38	48														
18	38	38	38	38	38	38	I5	38	38	38	38	38	I6	38	38	38	38	43													
19	38	38	38	38	38	38	I5	38	38	38	38	38	I6	38	38	38	38	38	43												
20	I5	I5	I5	I5	I5	I5	3I	I5	I5	I5	I5	I5	I5	I5	I5	I5	I5	I5	I5	4I											
21	38	38	38	38	38	38	I5	38	38	38	38	38	I6	38	38	38	38	38	38	I5	48										
22	I5	I5	I5	I5	I5	I5	3I	I5	I5	I5	I5	I5	I5	I5	I5	I5	I5	I5	I5	I5	I5	4I									
23	38	38	38	38	38	38	I5	38	38	38	38	38	I6	38	38	38	38	38	38	I5	38	I5	48								
24	I5	I5	I5	I5	I5	I5	3I	I5	I5	I5	I5	I5	I5	I5	I5	I5	I5	I5	I5	I5	3I	I5	3I	I5	4I						
25	38	38	38	38	38	38	I5	38	38	38	38	38	I6	38	38	38	38	38	38	I5	38	I5	38	I5	43						
26	38	38	38	38	38	38	I5	38	38	38	38	38	I6	38	38	38	38	38	38	I5	38	I5	38	I5	38	55					
27	38	38	38	38	38	38	I5	38	38	38	38	38	I6	38	38	38	38	38	38	I5	38	I5	38	I5	38	38	48				
28	38	38	38	38	38	38	I5	38	38	38	38	38	I6	38	38	38	38	38	38	I5	38	I5	38	I5	38	38	38	48			
29	38	38	38	38	38	38	I5	38	38	38	38	38	I6	38	38	38	38	38	38	I5	38	I5	38	I5	38	38	38	38	48		
30	38	38	38	38	38	38	I5	38	38	38	38	38	I6	38	38	38	38	38	38	I5	38	I5	38	I5	38	38	38	38	38	49	
31	38	38	38	38	38	38	I5	38	38	38	38	38	I6	38	38	38	38	38	38	I5	38	I5	38	I5	38	38	38	38	38	49	

Covariance matrix of  $\bar{v}_p$  measurements for  $^{237}\text{Np}$  (values,  $10^{-2}$ )

Table 4

Ser. No.	1	2	3	4	5	6	7	8	9	10	11	12	13	14	15	16	17	18	19	20	21	22	23	24	25	26	27	28	29	30	31			
1	100																																	
2	32	100																																
3	50	30	100																															
4	41	25	39	100																														
5	48	29	46	38	100																													
6	50	30	48	39	46	100																												
7	14	8	13	11	13	13	100																											
8	43	26	41	33	39	41	11	100																										
9	55	33	53	43	51	53	15	45	100																									
10	49	30	46	38	45	46	13	40	52	100																								
11	53	32	50	41	49	50	14	43	56	49	100																							
12	58	35	55	45	53	56	15	48	61	54	59	100																						
13	15	9	14	11	13	14	9	12	16	14	15	16	100																					
14	49	30	47	39	45	47	13	41	52	46	50	55	14	100																				
15	58	35	55	45	53	56	15	48	61	54	59	65	16	55	100																			
16	58	35	55	45	53	56	15	48	61	54	59	65	16	55	64	100																		
17	48	30	46	38	45	46	13	40	51	45	49	54	14	46	54	54	100																	
18	51	31	49	40	47	49	14	42	54	48	52	57	14	48	57	57	48	100																
19	55	34	53	43	51	53	15	45	58	51	56	61	16	52	61	61	51	54	100															
20	19	11	18	15	17	18	25	15	20	17	19	21	12	18	21	21	17	18	20	100														
21	49	30	47	39	45	47	13	41	52	46	50	55	14	47	55	55	46	48	52	18	100													
22	21	13	20	16	19	20	27	17	22	19	21	23	13	19	23	23	19	20	22	18	19	100												
23	49	30	47	39	46	47	13	41	53	46	50	55	14	47	55	55	46	49	52	18	47	20	100											
24	20	12	19	15	18	19	26	16	21	18	20	22	13	19	22	22	18	19	21	35	19	39	19	100										
25	55	34	53	43	51	53	15	46	59	52	56	62	16	52	62	62	52	55	59	20	52	22	53	21	100									
26	50	30	48	39	46	48	13	41	53	47	51	56	14	47	56	56	47	49	53	18	47	20	48	19	53	100								
27	51	31	49	40	47	49	14	42	54	48	52	57	14	48	57	57	48	50	54	18	48	20	49	19	54	49	100							
28	45	27	43	35	42	43	12	37	48	42	46	50	13	43	50	50	42	44	48	16	43	18	43	17	48	43	44	100						
29	48	29	46	38	44	46	13	40	51	45	49	54	14	46	54	54	45	47	51	17	46	19	46	18	51	46	47	42	100					
30	44	27	42	34	40	42	12	36	47	41	45	49	13	42	49	49	41	43	47	16	42	17	42	17	47	42	43	38	41	100				
31	45	28	43	35	42	43	12	37	44	42	46	50	13	43	50	50	42	44	48	16	43	18	43	17	48	44	44	39	42	38	100			

Table 3

Results of  $\bar{\nu}_p$  measurements for  $^{237}\text{Np}$  and statistical measurement error, relative units

Ser. No.	Neutron energy, MeV	$\bar{\nu}_p$	Square of statistical error, $S \cdot 10^{-4}$	Ser. No.	Neutron energy, MeV	$\bar{\nu}_p$	Square of statistical error, $S \cdot 10^{-4}$
I	0,98	2,795	0,18	I7	2,31	2,944	0,36
2	I,I7	2,815	0,44	I8	2,43	2,960	0,32
3	I,28	2,774	0,25	I9	2,62	2,981	0,22
4	I,38	2,772	0,64	20	2,64	3,011 <sup>x</sup>	0,53
5	I,46	2,824	0,32	21	2,71	2,990	0,34
6	I,62	2,817	0,35	22	2,79	3,003 <sup>x</sup>	0,36
7	I,66	2,907 <sup>x</sup>	I,29	23	2,92	3,006	0,32
8	I,68	2,882	0,25	24	3,07	3,051 <sup>x</sup>	0,43
9	I,77	2,841	0,20	25	3,09	3,065	0,21
I0	I,89	2,887	0,40	26	3,21	3,040	0,24
II	I,92	2,886	0,13	27	3,45	3,110	0,28
I2	2,00	2,853	0,19	28	3,52	3,084	0,49
I3	2,00	2,893 <sup>xx</sup>	I,38	29	3,71	3,166	0,30
I4	2,09	2,880	0,34	30	5,58	3,445	0,53
I5	2,13	2,878	0,11	31	5,90	3,493	0,48
I6	2,23	2,944	0,16				

\*/ Values obtained using fission chambers containing a smaller amount of fissionable material.

\*\*/ Results of measurements carried out using a spiral fission chamber.